AGU PUBLICATIONS

Geochemistry, Geophysics, Geosystems

RESEARCH ARTICLE
10.1002/2017GC007199

Modeling Slab-Slab Interactions: Dynamics of Outward Dipping Double-Sided Subduction Systems

Ágnes Király[1,2], Adam F. Holt[3], Francesca Funiciello[1], Claudio Faccenna[1], and Fabio A. Capitanio[4]

[1]Laboratory of Experimental Tectonics, Department of Sciences, Università degli Studi Roma Tre, Rome, Italy, [2]The Centre for Earth Evolution and Dynamics, University of Oslo, Oslo, Norway, [3]Earth, Atmospheric and Planetary Sciences, Massachusetts Institute of Technology, Cambridge, MA, USA, [4]School of Earth, Atmosphere and Environment, Monash University Clayton, Melbourne, VIC, Australia

Abstract Slab-slab interaction is a characteristic feature of tectonically complex areas. Outward dipping double-sided subduction is one of these complex cases, which has several examples on Earth, most notably the Molucca Sea and Adriatic Sea. This study focuses on developing a framework for linking plate kinematics and slab interactions in an outward dipping subduction geometry. We used analog and numerical models to better understand the underlying subduction dynamics. Compared to a single subduction model, double-sided subduction exhibits more time-dependent and vigorous toroidal flow cells that are elongated (i.e., not circular). Because both the Molucca and Adriatic Sea exhibit an asymmetric subduction configuration, we also examine the role that asymmetry plays in the dynamics of outward dipping double-sided subduction. We introduce asymmetry in two ways; with variable initial depths for the two slabs ("geometric" asymmetry), and with variable buoyancy within the subducting plate ("mechanical" asymmetry). Relative to the symmetric case, we probe how asymmetry affects the overall slab kinematics, whether asymmetric behavior intensifies or equilibrates as subduction proceeds. While initial geometric asymmetry disappears once the slabs are anchored to the 660 km discontinuity, the mechanical asymmetry can cause more permanent differences between the two subduction zones. In the most extreme case, the partly continental slab stops subducting due to the unequal slab pull force. The results show that the slab-slab interaction is most effective when the two trenches are closer than 10–8 cm in the laboratory, which is 600–480 km when scaled to the Earth.

Key Points:
- In outward dipping double-sided subduction, slabs can affect each other via mantle flow or by forces transmitted through the lithosphere
- Interaction can happen via mantle flow if the distance between the two trenches is smaller than ~500 km
- Initial geometric asymmetry disappears, while asymmetry due to preexisting mechanical heterogeneities in the plate intensifies over time

Supporting Information:
- Supporting Information S1
- Data Set S1

Correspondence to:
Á. Király,
agnes.kiraly@geo.uio.no

Citation:
Király, Á., Holt, A. F., Funiciello, F., Faccenna, C., & Capitanio, F. A. (2018). Modeling slab-slab interactions: Dynamics of outward dipping double-sided subduction systems. *Geochemistry, Geophysics, Geosystems*, *19*. https://doi.org/10.1002/2017GC007199

Received 25 AUG 2017
Accepted 27 JAN 2018
Accepted article online 5 FEB 2018

1. Introduction

The subduction of negatively buoyant lithospheric plates is the main driving mechanism of plate tectonics (e.g., Forsyth & Uyeda, 1975). Subduction evolution is composed of a variety of processes, ranging from fluid migration and the hydration of mantle rocks, which leads to arc volcanism, to the motions of the subduction trench, which results in upper plate deformation. However, seismicity and seismic tomography offer the only direct evidence of the current size, geometry and the deformation of the down-going slab. While many subduction properties can be readily understood in the context of single slab subduction evolution, dips and shapes in many complex tectonic regions are not reconciled in this simplified framework (e.g., Hayes et al., 2012; Heuret & Lallemand, 2005; Jarrard, 1986), which suggests that interactions with the mantle and neighboring slabs may play an important role (Di Leo et al., 2014; Holt et al., 2017; Király et al., 2016).

Numerical and laboratory models are a key-tool in developing our understanding of subduction evolution over geological time, specifically when integrated with seismological and geological data. In particular, many laboratory analog and numerical models addressed aspects of the subduction process that are relevant to double subduction geometries, for example, slab and trench migrations (Faccenna et al., 2007; Funiciello et al., 2003, 2004; Schellart, 2004; Stegman et al., 2006), and the 3-D mantle flow associated with the subduction (Funiciello et al., 2003, 2006; Jadamec & Billen, 2010; Piromallo et al., 2006). While these modeling studies substantially improved our understanding of the subduction process, there are a number of observations that are not yet well reproduced. Among these, mantle flow around single slabs is, in models, perpendicular to the trench toward the center of the subduction zone (above and below the slab), while near the slab edges the flow turns toward a more trench-parallel direction (e.g., Faccenda & Capitanio, 2012;

Long, 2013). However, these flow directions are not easily reconciled with observations, and may be affected by tectonic complexities, such as the presence of nearby slabs, slab windows or mantle plumes (e.g., Burkett & Billen, 2009; Di Leo et al., 2014; Druken et al., 2014; Guillaume et al., 2010; Király et al., 2016; MacDougall et al., 2014; Mériaux et al., 2015; Porritt et al., 2014; Salimbeni et al., 2013).

To date only a few studies investigate how multiple subducting slabs affect each other's dynamic evolution in an outward dipping subduction configuration, either via mantle circulation and/or stresses propagating through the rigid lithosphere (Di Leo et al., 2014; Holt et al., 2017; Zhang et al., 2017). Previous numerical models by Di Leo et al. (2014) showed that a double-sided subduction system, relative to a single subducting lithosphere, exhibits major differences in the mantle circulation and, in turn, the mantle's seismic anisotropy. So far, several important aspects of slab-slab interactions remained unaddressed including the role of heterogeneities within the lithosphere in double subduction systems.

In this paper, we focus on outward dipping double-sided subduction, i.e., slabs that dip away from each other on two sides of the same plate. This tectonic configuration can be found in several places on Earth, such as the Molucca and the Celebes Sea in the Philippine region or the Adria plate in the Mediterranean (Figure 1). We use laboratory and numerical models to study the geometry, motions and evolution of double-sided subduction systems and the related mantle flow. The combined modeling approach allows to overcome unavoidable limitations that characterize both approaches, and to better explore the parameter space of the studied process. The goal of the study is to examine the effects of slab-interaction between two oppositely dipping subduction zones that are attached to the same plate, both in the case of a symmetric initial subduction configuration, and in systems where asymmetry is present (Figure 2). We firstly characterize the kinematic expression of symmetric outward dipping double-sided subduction, relative to single slab subduction models with equivalent properties. Then, we consider the role of two forms of asymmetry on the dynamics of outward dipping double-sided subduction, to test how asymmetry affects the overall subduction kinematics on both sides of the plate, and how the perturbation evolves over the subduction history. Asymmetry is introduced into the subducting plate in the following two ways; variable initial depths for the two subducting slabs ("geometric" asymmetry), and variable buoyancy within the subducting plate (i.e., a continent: "mechanical" asymmetry). For the subset of models with mechanical

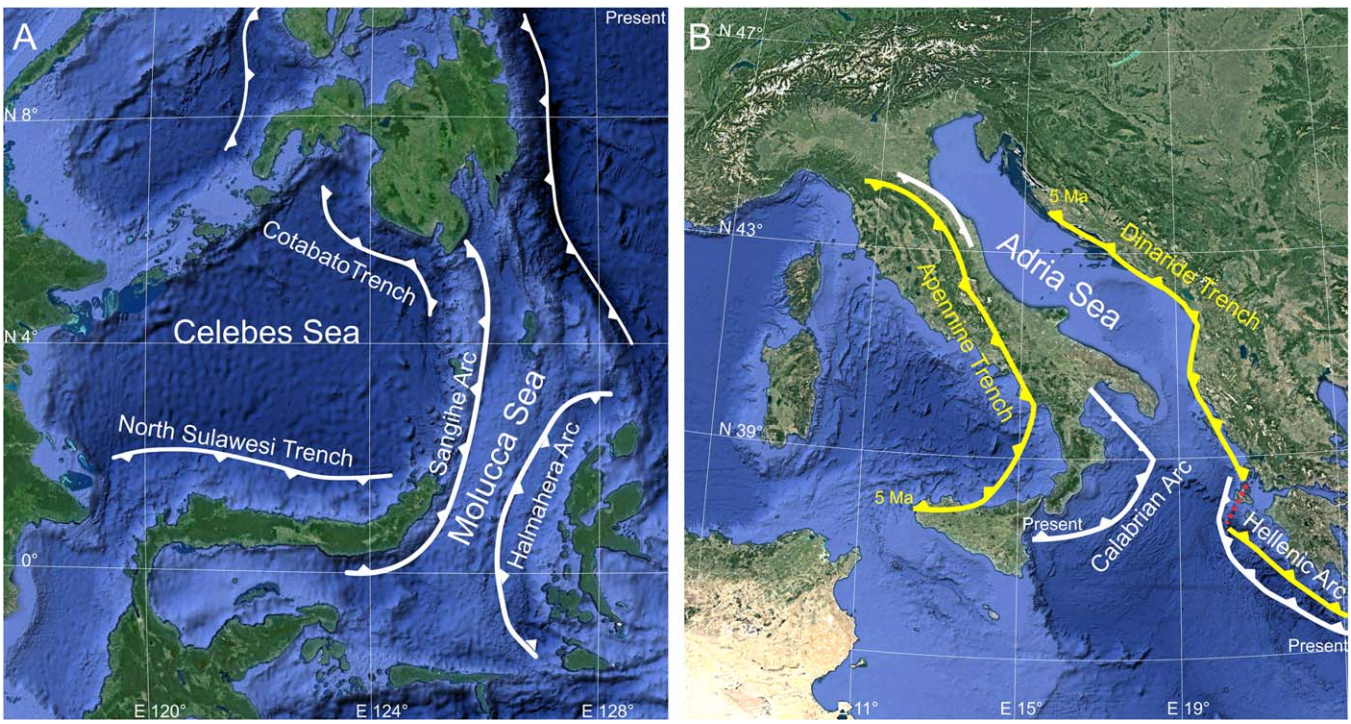

Figure 1. Position of trenches in different areas of double-sided subduction zones. (a) Present-day situation of the Molucca and the Celebes Sea subduction zones (mod. after Di Leo et al., 2012). (b) Subduction zones on the two sides of Adria plate 5 Ma (orange) and in present days (white) (mod. after Faccenna et al., 2014a).

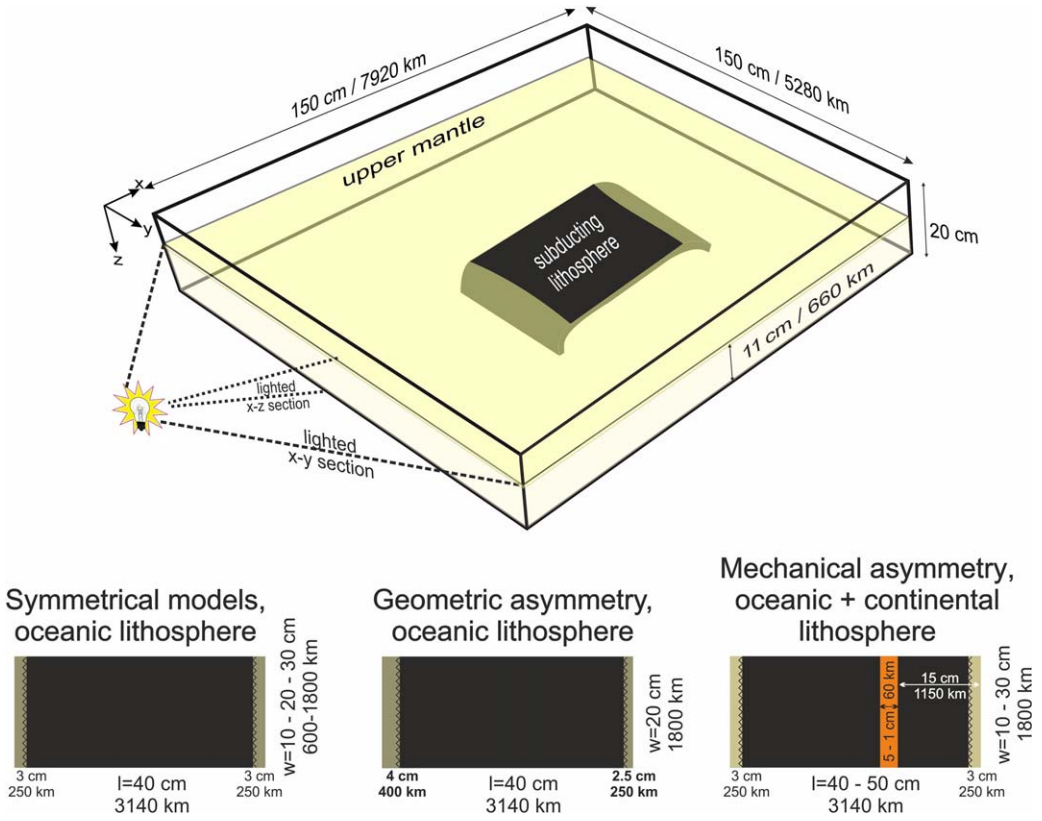

Figure 2. General setup of the outward dipping double-sided subduction models. In the laboratory, the mantle is lighted in the top 1 cm layer, to track the horizontal mantle flow. At the bottom, we show the top view sketches of the three different tested scenarios.

asymmetry, we additionally examine the role of the initial slab separation (trench perpendicular plate length), and the plate width (trench-parallel).

These asymmetric cases offer new insights into natural tectonic settings, such as those in South-East Asia at the Molucca Sea and in the Mediterranean, along the sides of the Adria plate (Figure 1; e.g., Djajadihardja et al., 2004; Faccenna et al., 2014a) respectively, where, different depths of subduction (geometrical asymmetry) and continental block subduction (mechanical asymmetry) on both sides of the plates occur. By gradually increasing the complexity of the models throughout our study, and using an approach that combines laboratory models with numerical models, we strive to develop a holistic view of the dynamics underlying double-sided subduction in an outward dipping geometry.

2. Model Definition

In the following section, we first describe the assumptions embedded within the design of the laboratory and numerical models, and then describe an exemplary setup used in the two different approaches for modeling outward dipping double-sided subduction. We finally illustrate the force balance expected in such models.

2.1. Assumptions

Our laboratory and numerical models are set up in the following framework: (1) subduction evolves self-consistently, driven only by the negative buoyancy of the oceanic lithosphere, while no external kinematic boundary conditions (i.e., plate or trench velocity) are imposed. (2) The box boundaries are assumed as the reference frame. (3) The materials deform with an effective linear viscous rheology. (4) The system is isothermal. Hence, thermal diffusion, phase changes, and temperature-dependent density and viscosity change are neglected. Temperature-dependent density is implemented as a constant density contrast. Hence, the

slab is considered to be in a quasi-adiabatic state, which is justified by the high model subduction velocities (>1 cm yr^{-1}). (5) The system does not include an overriding plate, which implicitly assumes that it passively moves along with the trench and that the subduction interface has the same strength as the upper mantle. While this assumption influences the rate of trench migration, it does not affect the overall behavior (e.g.,van Dinther et al., 2010, Holt et al., 2015; Yamato et al., 2009). (6) For the sake of simplicity, we study the evolution of slabs only in the upper mantle, and so the upper-lower mantle discontinuity is modeled as an impermeable boundary.

2.2. Laboratory Model Setup and Experimental Procedure

Following the approach used in previous analog laboratory models (Faccenna et al., 2001; Funiciello et al., 2003; Guillaume et al., 2013), subduction is modeled in a linearly viscous two-layered system hosted in a 150 × 150 × 20 cm^3 sized Plexiglas tank. The tank is filled with an 11 cm high layer of low-viscosity and high density glucose syrup, a Newtonian fluid with a viscosity in order of 10^3 Pa s (Table 1), which simulates the upper mantle. On the top of the syrup we put a silicone putty plate as the lithosphere analogue. The silicon putty is made of Polydimethylsiloxane mixed with iron fillers, which allow us to tune its viscosity and density. This has the rheology of a viscoelastic material, with viscous behavior at strain rates below ~0.1 s^{-1} (Weijermars & Schmeling, 1986). For the applied experimental strain rates, the silicone putty can be thus considered as a quasi-Newtonian highly viscous (~40,000 Pa s) fluid where stress increases linearly with strain rate (Boutelier et al., 2008; Weijermars & Schmeling, 1986). As Newtonian materials have a more resistant response to deformation than power-law fluids (Ranalli, 1995), the velocities observed in the laboratory should be considered as a lower bound. The material properties and scaling factors are summarized in Table 1. These materials fulfill the standard scaling procedure for stresses to density, viscosity and length under the natural gravity field (see in Table 1; Boutelier & Cruden, 2008; Davy & Cobbold, 1991; Funiciello et al., 2003; Hubbert, 1937; Weijermars & Schmeling, 1986).

The experimental procedure requires the positioning of the silicone plate on the top of the syrup, and, after a short relaxation time, subduction is synchronously initiated at the two opposite margins of the plate. In most of the models (except those with geometrical asymmetries) both of the two tips of the silicone plate are forced into the syrup to a depth of about 3 cm, which is equal to 180 km in nature (see in Table 1 and Figure 2). This creates enough negative buoyancy to sustain self-driven subduction. The models finish when the two trenches reached a separation distance of ~3–2 cm (equal to 180–120 km in the natural prototype).

Table 1
Physical and Scaling Parameters of Laboratory and Numerical Experiments[a]

	Parameters	Unit	Nature	Laboratory model	Numerical model
g	Gravitational acceleration	m s^{-2}	9.81	9.81	9.81
Thickness		m			
h_{sp}	Oceanic lithosphere		100,000	0.014	80,000
h_{co}	Continental lithosphere		100,000	0.014	80,000
h_{um}	Upper mantle		660,000	0.1	660,000
	Scale factor for length		L_{model}/L_{nature}	~1.52 × 10^{-7}	
Buoyancy		kg m^{-3}			
$\rho_{sp}-\rho_{um}$	Oceanic lithosphere		~60	79	62.5
$\rho_{op}-\rho_{um}$	Continental lithosphere		~−50	−41	−40
Viscosity		Pa s			
η_{sp}	Subducting oceanic plate		10^{22}–10^{23}	~4 × 10^4	2 × 10^{22}
η_{op}	Overriding plate		10^{23}–10^{24}	~3 × 10^4	2 × 10^{22}
η_{um}	Upper mantle		10^{20}	~200	10^{20}
	Viscosity ratio		η_{oc}/η_{um}	~200	200
Reynold number	$Re = v \cdot l \cdot \Delta\rho \cdot \eta^{-1} \ll 1$		10^{-21}	10^{-6}	10^{-21}
Scaling of time	$(t_{nature}/t_{model}) = ((\Delta\varrho gh)_{model}/(\Delta\varrho gh)_{nature}) \cdot (\eta_{nature}/\eta_{model}))$		3.16 × 10^{13} (1 Myr)	~60 s	
Scaling of velocity	$(U_{model}/U_{nature}) = (t_{nature} \cdot L_{model})/(t_{model}/L_{nature})$		1 cm/yr	1.5 mm/min	

[a]With these parameters we fulfil the geometric, kinematic, and dynamic similarity criteria (Hubbert, 1937).

Each model is monitored with a sequence of photographs taken at regular time intervals (30 s) in top and oblique/lateral views. The top view images are used to track trench and plate motion, as well as the horizontal component of the mantle flow. The latter is calculated using the Particle Image Velocimetry technique (i.e., PIVlab software; Thielicke & Stamhuis, 2014). The oblique view photos are used to monitor the overall system, with a specific focus on the slab dip angle. Similarly to Bellahsen et al., (2005), the experimental time and velocities (both in the laboratory and the numerical results) are normalized by the time taken for the slab to arrive at the bottom and with a characteristic velocity derived from Stokes equation, which is calculated as:

$$V_{ch} = \Delta\rho \cdot g \cdot h_{sp} \cdot h_{um} / \eta_{um} \quad (1)$$

where $\Delta\rho$ is the density difference between the slab and the mantle, g is the natural gravitational acceleration, h_{sp} is the thickness of the subducting plate, h_{um} is the thickness of the upper mantle and η_{um} is the viscosity of the upper mantle.

2.3. Numerical Model Setup

We complement our laboratory approach with 3-D numerical models of double-sided subduction (Table 1 and Figure 2). We use the finite-element code CitcomCU to model incompressible Stokes flow in a 3-D, Cartesian domain (Moresi & Gurnis, 1996; Zhong, 2006). As in the laboratory models, we consider a purely Newtonian viscosity, and model lithospheric plates with a constant viscosity and constant density. The numerical model setup is derived from the "out-dip" model presented in previous work (Holt et al., 2017, section 4.2.1), but with a number of important differences in order to render the numerical models more comparable to the laboratory models. To first order, this requires the removal of the upper plates and the exclusion of the strong lithospheric core. Additional modifications are implemented in order to generate a numerical model setup with plate geometry, plate-mantle viscosity and density contrasts, close to the laboratory experiments (see Table 1 for a complete description of parameters).

Despite these efforts, the numerical models differ slightly from the laboratory ones, particularly in terms of boundary conditions. Unlike the free surface in the laboratory models, the upper boundary of the numerical models is free-slip and so a weak "crustal" layer is required to decouple the subducting slab from the upper boundary (e.g., Quinquis et al., 2011). A 15 km thick layer, with viscosity equivalent to that of the asthenosphere, is therefore embedded in the top portion of the 80 km thick subducting plate. The mechanical boundary conditions of the bottom and the sidewalls of the system are not trivial to categorize in the analog models, where a layer of glucose syrup is adjacent to the Plexiglas bottom and sidewalls, resulting in an intermediate boundary condition between mechanical free- and no-slip. This condition allows the slab tip to slightly move laterally on the basal boundary. We therefore run numerical models with both no- and free-slip bases, i.e., both end-members, but chose to focus on the models with the free-slip base.

2.4. Background on Forces in the Modeled Subduction System

In the models presented here, the only driving force is the slab pull, provided by the negative buoyancy of the lithosphere. On the other hand, a number of resistive forces contribute to the overall dynamics of the system: (1) The plate has an internal bending resistance (F_b), which is proportional to the plate's viscosity and the cube of the ratio of the plate's thickness and its curvature($\sim\eta_l \cdot (h_l/R)^3$), (e.g., Conrad & Hager, 1999). (2) Additionally, an internal viscous resistance prevents in-plane stretching of both the slab and the plate. (3) Slab sinking is resisted by a shear drag on its interface (F_{sh}), which is a function of mantle viscosity, subduction velocity and surface area of the slabs. The shear resistance acts also at the bottom of the lithosphere (basal shear, F_{bs}), which tends to prevent the plate motion with respect to the box boundaries. (4) After the slabs interaction with the 660 km discontinuity, a frictional force is exerted on the slab by the bottom boundary of the box, where it is partially anchored. In addition, (5) there is a pressure force directed toward the mantle wedge side of the slab, driven by mantle flow in both the mantle wedge and the sub-slab mantle. This force is proportional to both the pressure difference across the slab (ΔP) and the slab length ($F_{dp} \approx \Delta P \times$ slab length). In the double-sided configuration, we have to account for a highly time-dependent F_{dp}. As the two slabs get closer together, the pressure in the sub-slab mantle

(i.e., between the two slabs) increases, thereby resulting in an increase in the magnitude of ΔP, and therefore F_{dp} (Holt et al., 2017).

3. Results

Here, we present the results of three sets of models characterized by: a) a homogenous oceanic (i.e., negatively buoyant) lithosphere (i.e., symmetric models); and b) initial geometric asymmetry with different initial slab depths on the two sides, and c) mechanical asymmetry with a composite plate containing a stripe of buoyant continental lithosphere on one side of the plate (Figure 2 and Table 2).

We first describe some experimental single subduction models, which serve as a reference for the double-sided subduction models. The reference models were performed either with a homogeneous oceanic plate or with a subducting plate that consists of heavy oceanic and buoyant continental parts (i.e., inhomogeneous plate). We subsequently describe the laboratory double-sided subduction models in conjunction with the double-sided numerical models that fall into the three categories listed above.

The experimental results are derived from 25 models (Table 2), including 12 double-sided- and 13 single subduction models. In the numerical modeling sections, we examine a more limited number of models: aligned with the first set of analog models (i.e., homogeneous models), we test two different plate widths and free/no-slip basal boundary in a symmetrical setup. In the asymmetric section, we modify the numerical model that is most comparable to the analog models (w = 1,800 km, free slip bottom) to introduce asymmetry in two following ways that align with the workflow adopted for the laboratory analog models: i) the two initial slab depths are different (geometric asymmetry), ii) a strip of light, continental material is embedded within the otherwise oceanic plate at a distance of 360 km from the plate center (mechanical asymmetry).

Table 2
List of Experiments[a]

		Width (cm)	Length (cm)
Homogenous oceanic plate			
Adria00a	Single subduction, fixed trailing edge	10	40
Adria00b	Single subduction, fixed trailing edge	30	40
Adria04a	Single subduction, free trailing edge	10	40
Adria04b	Single subduction, free trailing edge	30	40
Adria02b	Double subduction	10	40
Adria03a	Double subduction	20	40
Adria13	Double subduction	30	41
Adriax3	Double subduction (lateral view)	30	40
Adria03c	double subduction (geometric asymmetry)	20	40
Inhomogeneous plate			
Adria05d	Single subduction, oceanic + continental, fixed trailing edge	10	15 + 25
Adria05c	Single subduction, oceanic + continental, fixed trailing edge	30	15 + 25
Adria12	Single subduction, oceanic + continental, free trailing edge	10	15 + 25
Adria05b	Single subduction, oceanic + continental, free trailing edge	30	15 + 25
Adria07a	Single subduction, oceanic + continental + oceanic, fixed trailing edge	10	15 + 1 + 25
Adria07b	Single subduction, oceanic + continental + oceanic, fixed trailing edge	30	15 + 1 + 25
Adria11	Single subduction, oceanic + continental + oceanic, free trailing edge	10	15 + 1 + 25
Adria20	Single subduction, oceanic + continental + oceanic, free trailing edge	10	15 + 1 + 25
Adria21	Single subduction, oceanic + continental + oceanic, free trailing edge	30	15 + 1 + 26
Adria10	Double subduction, oceanic + continental + oceanic (mechanical asymmetry)	10	15 + 1 + 25
Adria08a	Double subduction, oceanic + continental + oceanic ("short model" with mechanical asymmetry)	10	15 + 1 + 25
Adria08b	Double subduction, oceanic + continental + oceanic (mechanical asymmetry)	30	15 + 1 + 25
Adria09a	Double subduction, oceanic + continental + oceanic ("long model" with mechanical asymmetry)	10	15 + 1 + 35

[a]The trench kinematics of Adria 00a, 00b, 4a, 04b, 02b, and 13 and the toroidal and poloidal flow pattern from Adria 03a and x3 are shown in Figure 3. Figure 4 shows results of Adria 02b, 03a, and 00a. The initial phase of Adria 03c is shown in Figure 5, while Figure 6 shows results from Adria 07a, 20, 08a, and 09a.

3.1. Reference Single Slab Subduction Models

3.1.1. Homogeneous Plate

The far-field boundary conditions of single subduction models have two end-members: one where the trailing edge of the subducting plate is fixed, the other with a free subducting plate. This either maximizes or minimizes the slab roll-back, respectively, and allows or inhibits plate absolute motions and influences the induced mantle circulation during subduction (Funiciello et al., 2004). Here we use both of these two end-members as a reference for the more complex double-sided subduction models.

Despite the trailing edge condition, the subduction process always evolves through the following three distinct phases (e.g., Bellahsen et al., 2005; Funiciello et al., 2004) (Figure 3): (1) the slab sinks into the mantle while the dip angle is progressively increasing. The geometrical and rheological characteristics of our models always produce slab roll-back (Bellahsen et al., 2005). During this phase, the rate of trench retreat increases with time and with the amount of subducted material. (2) The slab interacts with the impermeable bottom boundary layer, causing a slow-down in trench velocity and a slight decrease of dip. (3) A steady state phase during which the trench velocity and slab dip are constant. In this phase, the normalized velocity of trench retreat (i.e., trench velocity divided by Stokes velocity) is quasi-constant and equal to about 0.01 when the plate is fixed at the trailing edge, independent of the plate width. In contrast, when the plate is free, the trench retreat becomes slower and is influenced by the plate's width. The narrow (10 cm; i.e., 600 km scaled to nature) and the wide (30 cm; 1,800 km scaled to nature) free plates show a normalized trench velocity of about 0.007 and 0.005, respectively (Figures 3c and 3d), in agreement with previous modeling results by Stegman et al. (2006) as well as by Strak and Schellart (2016).

The free trailing edge condition allows the plate to move toward the trench. For the narrow subducting plate, the rate of plate motion grows concurrently with the trench retreat velocity during the free sinking phase. However, as the slab interacts with the base, the plate velocity decreases, and during the steady state subduction, is lower than the trench retreat velocity. With a wider subducting plate, the plate motion is initially greater than the trench retreat rate, but during the steady state phase they are approximately equal.

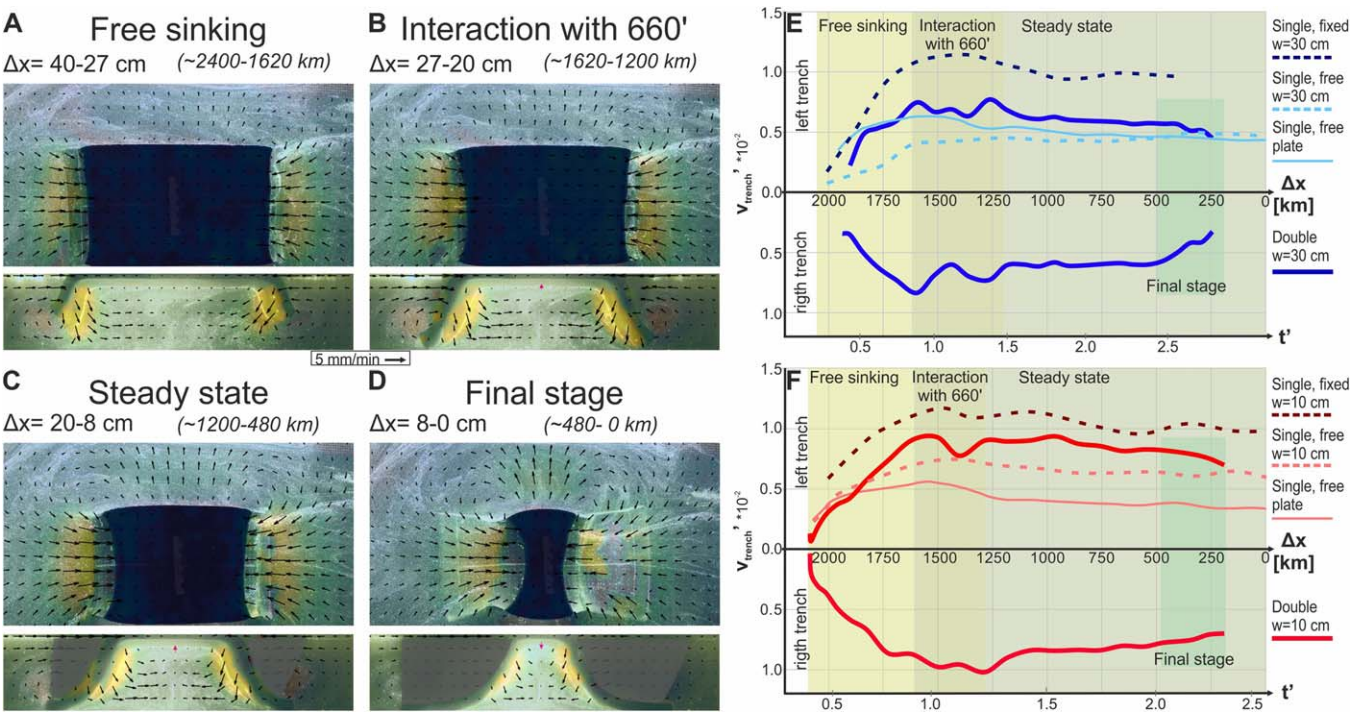

Figure 3. Evolution of the homogenous models. (a–d) Top and lateral view photos with mantle velocity in four representative times from the models Adria 03a and Adria_x3, respectively. (e and f) Normalized trench velocities of 30/10 cm wide single- and double-sided subductions (data from the following models: Adria 00a, 00b, 04a, 04b, 02b, and 13).

The subduction process triggers a complex 3-D, time-dependent mantle circulation pattern. As already extensively described in previous experimental works (e.g., Funiciello et al., 2003; Funiciello et al., 2004, 2006; Kincaid & Griffiths, 2003, 2004; Schellart, 2004, 2008; Strak & Schellart, 2014), the flow has poloidal and toroidal components since the beginning of subduction. The poloidal flow component is characterized by two cells, in the mantle wedge and sub-slab areas. The toroidal flow component consists of two cells centered on the lateral slab edges. The mantle circulation pattern is highly time-dependent and exhibits strong variations between the three phases. Both poloidal and toroidal velocities increase during the free falling of the slab into the upper mantle (phase #1) and then decrease when the slab approaches the 660 km discontinuity (phase #2). After the slab's interaction with the bottom, poloidal flow is reduced in the sub-slab domain, and the toroidal flux becomes dominant.

As observed in previous analog and numerical modeling studies (e.g., Funiciello et al., 2006, Piromallo et al., 2006), when the plate has a free trailing edge condition, and the rate of retreat is smaller, the toroidal flow amplitude reduces. In fact, when the rate of plate movement is greater or in the same range as the trench retreat velocity, the mantle flow dragged by the plate partly overwrites the vortex like flow around the slab edge to produce a more elongated toroidal cell with a reduced trench-parallel flow component.

3.1.2. Inhomogeneous Plate

Single subduction models with an inhomogeneous lithospheric plate were carried out as references for the double-sided subduction models with mechanical asymmetry. The inhomogeneous lithosphere is composed of sections of heavy oceanic and light continental lithosphere. First, we aimed to assess the maximum amount of subductable continental lithosphere, and so constructed preliminary models with an analog plate that consisted of a 15 cm long oceanic component and a 25 cm long continental component. We found that, depending on the trailing edge condition, a minimum of 2- and a maximum of 3 cm long stripe of continental lithosphere could enter into the subduction before the slab sinking stalled. Following the preliminary tests, we performed the inhomogeneous reference models with a plate in which 1 cm stripe of continental lithosphere was embedded between 15 and 25 cm long oceanic sections (Table 2). Again, two end-member trailing edge conditions have been tested: fixed and free.

Initially the inhomogeneous single subduction models evolve in a similar manner to the homogeneous reference models, going through an initial free sinking phase with increasing trench and subduction velocity, then a slow-down during the interaction with the bottom barrier, followed by a short phase of steady state subduction, which is later affected by the subduction of the 1 cm wide stripe of continental lithosphere. When the fixed trailing edge condition is imposed, the entry of the continent into the trench causes a decrease in subduction velocity by more than 50% (relative to the steady state velocity). However, subduction does not stop completely and the continental strip reaches the bottom of the box, after which the subduction transitions to a new steady state subduction, with a velocity that increases to the rate attained prior to continental subduction (Figure 7C). When the imposed trailing edge condition is free, the entry of the continent causes a smaller decrease rate of the subduction velocity (50% slower decrease than in the fixed model), which continues for a longer time, until it obtains a constant slow rate of $\sim$0.001 normalized subduction velocity ($\sim$0.25 mm/min). With this reduced rate, the continental stripe reached a depth of only 4 cm within 3 hours experimental time ($t'=9.7$).

In all of the single slab reference models, the mantle around the slab flows at a velocity that is consistent with the decrease and the re-acceleration of the trench motions.

3.2. Double-Sided Subduction of a Homogeneous Oceanic Plate

3.2.1. Results From Laboratory Models

The evolution of the two oppositely dipping oceanic slabs is ideally symmetrical, as it was shown in previous numerical results (Di Leo et al., 2014; Holt et al., 2017; Zhang et al., 2017). This was also observed in the laboratory models, in which the subducting slabs achieve symmetry during their evolution (Figure 3). As in the homogeneous single slab reference models, the two slabs go through the initial, free sinking phase with increasing subduction velocity, then the subduction velocity reduces as the slabs interact with the bottom barrier, and finally the slabs attain a near steady state phase (Figures 3a–3c). However, as the two slabs approach each other the steady state phase transforms into a fourth, "final stage" phase where the two slabs affect each other and the trench retreat motion slows down (Figure 3d).

Initially, the trench velocity is insensitive to the width of the subducting plates and, as in the reference models, it increases during the free sinking phase (#1) and slightly decreases during the interaction with the bottom boundary (i.e., the analog of the 660 km discontinuity). The magnitude of the trench velocities is intermediate between the rates within the reference models characterized by fixed and free trailing edges, respectively (Figures 3e and 3f). Once the slabs are anchored to the bottom, the retreat rate of the two trenches slowly decreases, resulting in a deceleration rate of $1.27–1.61 \cdot 10^{-6}$ normalized velocity/km, for narrow or wide plates, respectively, during a total of 800 km (13 cm in the laboratory) convergence between the two trenches. At the same time, narrow trenches generally migrate 35–40% faster than the wide ones. When the slabs approach each other to a distance of 540–480 km (i.e., 9–8 cm), the double-sided subduction transitions into its final stage, where the trench retreat rates further slow down with a deceleration rate of 2.93 normalized value/km for the narrow trenches and 7.34 normalized value/km for the wide trenches (Figures 3e and 3f). Due to the approximately symmetrical evolution of the two subduction zones, the center of the plate does not move with respect to the box boundaries. On the other hand, the plate itself undergoes a small amount of trench-perpendicular extensional deformation and some reduction in the plate width.

During homogeneous double-sided subduction, the subduction induced mantle flow evolves as follows (Figures 3a–3d): initially a very weak toroidal flow develops, similar to that within the single subduction models (Figure 3a), while in the vertical plane the mantle flows around the slab tips from the sub-slab to the mantle wedge area. After the slabs reach the bottom boundary, the flow in the two toroidal cells strengthens and an escape flow from below the plate develops with increasing velocity (Figures 3b–3d). The escape flow is a consequence of the continuous decrease in the volume of the sub-slab mantle. The poloidal flow in the sub-slab area has two distinct cells, with strong downwelling close to the slabs and a weak upwelling under the center of the plate (Figures 3b and 3c). As slabs approach, the two poloidal cells in the sub-slab area merge together, cancelling out the upward component of the flow and resulting in downwelling underneath the center of the plate (Figure 3d).

At the same time, the two toroidal cells also combine. This results in a more vigorous escape flow from below the plate, which results in the elongation of the toroidal flow cells in a trench-parallel direction (Figure 3). In Figure 4, we present the average escape flow rate against the separation distance between the two trenches (Δx) and the distance from the plate edge (Δy). This is calculated from the PIV results, by summing the amplitude of the horizontal velocity vectors between the two trenches (at a constant (Δy) distance from the plate edge) and dividing by the distance between the trenches (Δx). As the results depend on the quality of the PIV, we selected to display those models that are characterized by a similar number of vectors and signal/noise ratio.

We show the results of the homogeneous double-sided subduction models with 10 cm (Figure 4a) and 20 cm (Figure 4b) wide plates, respectively. The amplitude of the average escape flow rate is proportional to the plate width, i.e., in the model with w = 10 cm the maximum is 0.0035 1/s, while with w = 20 cm it is 0.0070 1/s. Additionally, both double-sided models have a flux density that is at least a factor of two greater than the 10 cm wide, fixed reference model (Figure 4e). The flow rate at a distance of 2–3 cm (scaled to 120–180 km) from the plate edge in the double-sided models (Figure 4e), has a greater increase in the escape flow with respect to the reference single slab model, since almost the beginning of subduction. Additionally, in the model with a 10 cm (i.e., 600 km) wide plate, the growth of the average escape flow rate further increases between ~500 and 300 km scaled horizontal trench separation, which corresponds to the time when the subduction transitions into its final stage and the deceleration of the trench retreat increases. This change in the growth rate of the escape flow is not observed with the wider (w = 20 cm/1,200 km) plate.

3.2.2. Results From Numerical Models

From the results of the symmetrical numerical models, we firstly describe the kinematics observed in the model with free-slip bottom boundary condition and a dimensional plate width equivalent to the 30 cm wide plate analog model (w = 1,800 km), as this model is most directly comparable to the analog experiments. We then describe the motions of models with narrower plates, and assess the impact of changing the bottom boundary condition to no-slip.

Similar to the laboratory models, the numerical models go through a four-phase evolution of subduction, with free-sinking, bending on top of the model base, and near-steady state with a final interacting phase with further slow-down in trench retreat. In addition, the rate of trench retreat is strongly time-dependent throughout the models (Figure 5c). After an initial increase in trench retreat before the slab-tip touches the

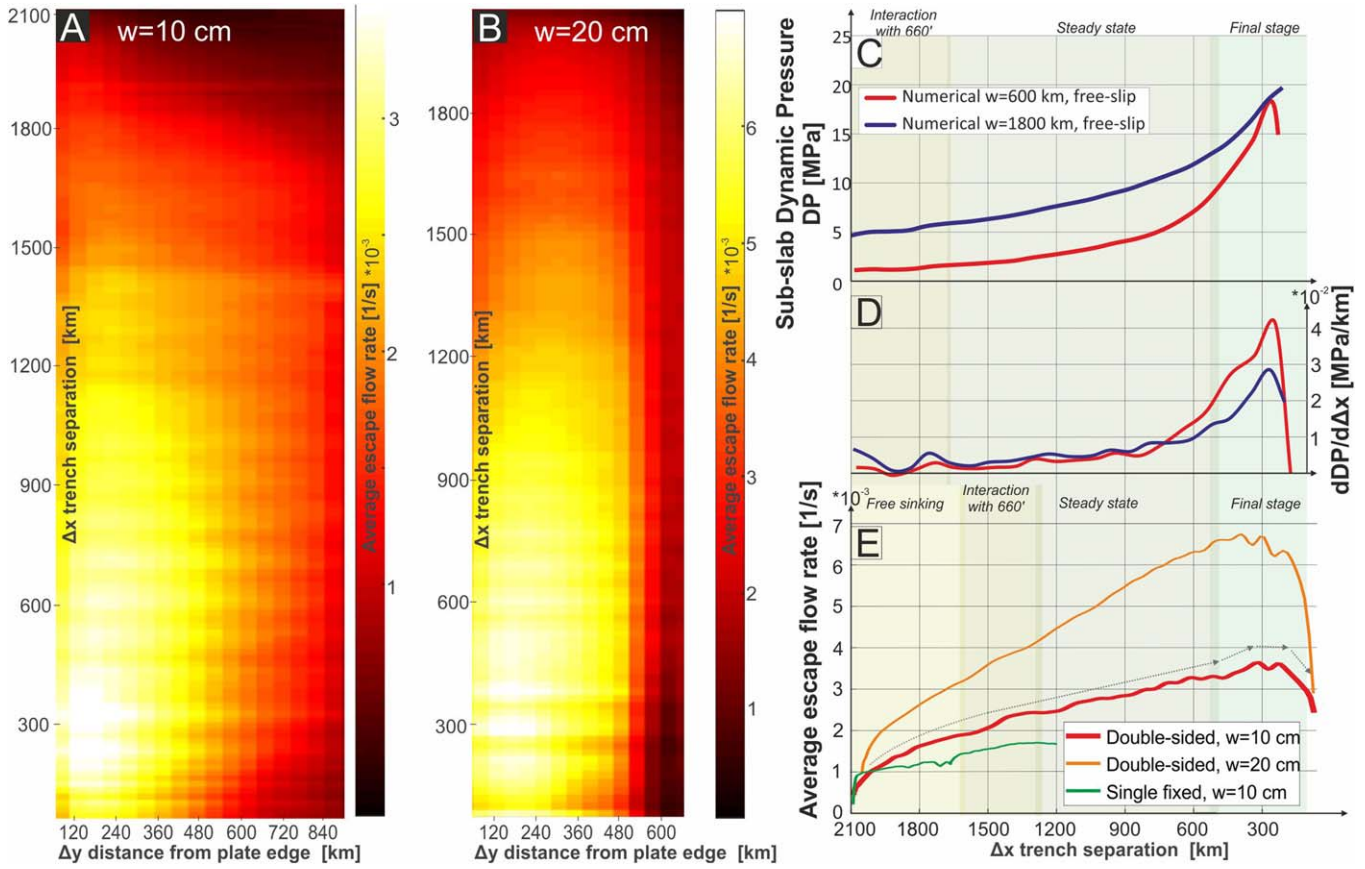

Figure 4. Average escape flow rate (in 1/s) in homogenous double-sided subduction models ((a) Adria 02b and (b) Adria 03a). The *x* axes represent the distance from the edge of the plate (Δy), while the *y* axes are the distance between the two trenches (Δx; i.e., time goes from top to bottom). Note that the color scale bar is different in the plots 4a and 4b. On Figure 4c, we show the increase of dynamic pressure in the subslab area, measure in the numerical models with free-slip bottom boundary condition. On Figure 4d, we plot the change of dynamic pressure in the numerical models (from Figure 4c), while Figure 4e shows the escape flow rate of the laboratory models (w = 10/20 cm and the reference single fixed model with w = 10 cm) Δy = 20–30 mm.

model base (i.e., during the free-sinking phase), the dominant trend is a decreasing trench retreat rate as the trenches become closer together. As the slabs reach the base, the trench retreat velocity decreases from a maximum normalized value (i.e., trench retreat rate normalized by the characteristic velocity; equation (1)) of 0.02 at a trench separation of 1,750 km to a normalized rate of 0.015 at a separation of 500 km (i.e., deceleration with a rate of $4{\cdot}10^{-6}$ normalized value/km). This is a more rapid decrease than the respective laboratory model (w = 30 cm, where the rate of deceleration is $2.8 \cdot 10^{-6}$ normalized value/km). In the last phase, the rate of trench retreat deceleration amplifies to $1.2{\cdot}10^{-5}$ normalized value/km (compared to $9.9{\cdot}10^{-6}$ normalized value/km in the laboratory model), which leads to a normalized trench retreat velocity of 0.012 at a trench separation of 250 km.

In the first phase, once the two initial slabs have subducted to mid-mantle depths ($z \sim$ 330 km), the slabs dip at angles of ≈70°, which then decreases to ≈65° as the model evolves into steady state subduction. The slab dip angle further decreases to 55–58°, when the two trenches reach a separation distance of ∼500 km. Holt et al., (2017) showed that the slab dip can be correlated with the across-slab difference in dynamic pressure (ΔP_d), as ΔP_d is approximately equal to slab buoyancy times the cosine of the slab dip angle. The dynamic pressure in the mantle can be directly extracted from the numerical models: In the sub-slab area, the dynamic pressure (P_d) shows an increasing trend as the slabs approach each other (Figures 4c and 5). This is accompanied by an increasingly negative pressure in the mantle wedge region, resulting in a growth of ΔP_d. For this reference model, P_d increases from a magnitude of ∼5 MPa (Δx = 2,500 km trench separation) to a value of ∼26 MPa as the slabs become very close (Δx = 250 km separation). As the mantle pressure is intrinsically coupled to the mantle flow, we found a good correspondence between the average

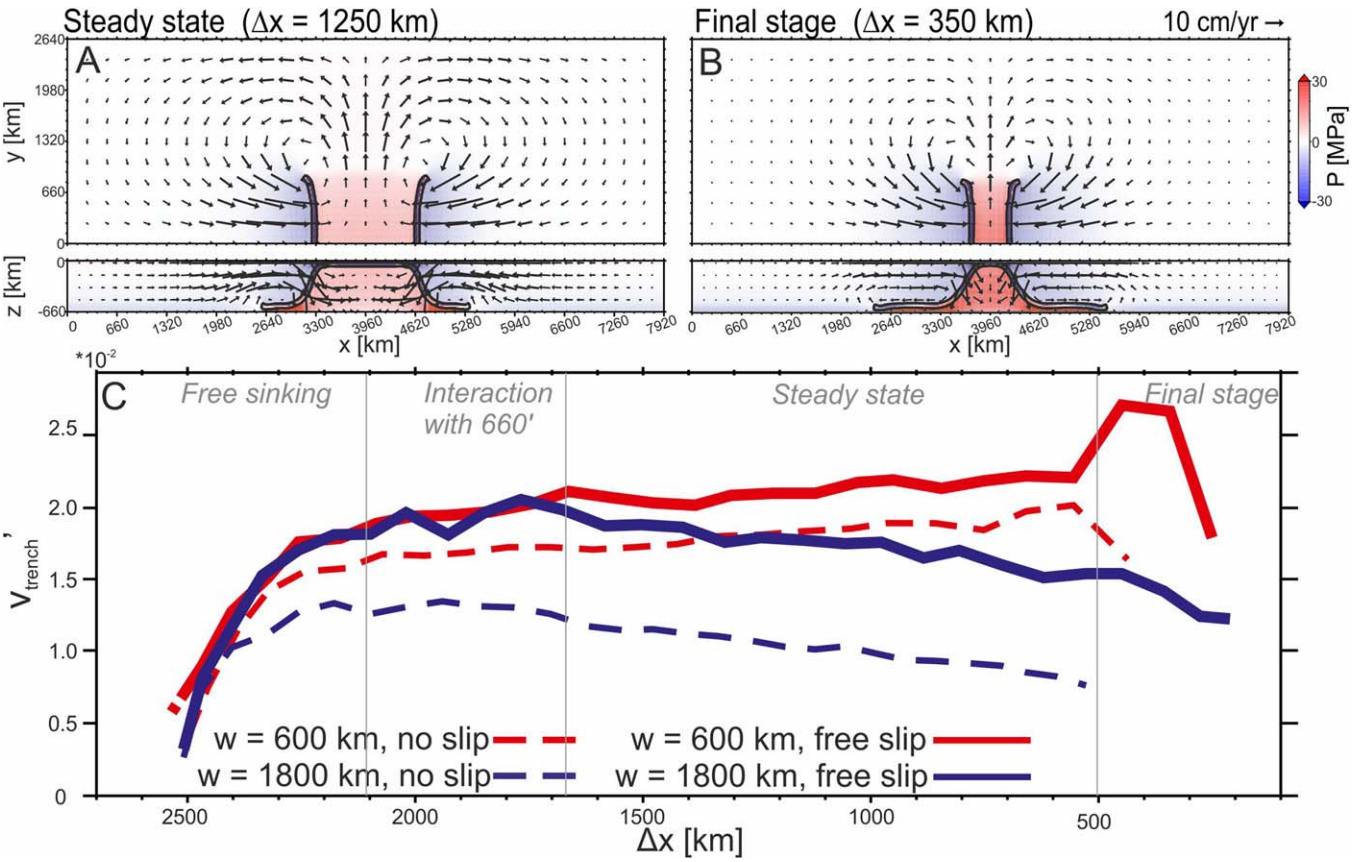

Figure 5. Evolution of the mantle pressure and trench retreat velocity in the homogenous double-sided numerical models, with variable plate width (600 km, 1,800 km) and basal boundary condition (free slip, no slip). (a and b) Snapshots of the mantle flow and dynamic pressure fields were taken at two representative times in the wide plate model with the free-slip bottom. The horizontal slices ($z = 330$ km), and trench-perpendicular vertical slices taken at the center of the subducting plate ($y = 0$). (c) Evolution of normalized trench retreat velocity.

escape flow rate in the laboratory models and the sub-slab dynamic pressure in the numerical models (Figure 4). In addition, we observe very similar mantle flow patterns, both in plan-view (i.e., toroidal) and side-view (i.e., poloidal), as those observed in the laboratory models and described in the previous section (cf. Figures 3a–3d, 5a, and 5b).

In addition to the reference numerical model described above, we have examined the role of variable plate widths ($w = 600$ km versus 1,800 km) as well as the basal boundary condition (i.e., no slip versus free slip), which can be tested only in the numerical models. For the original, wide plate model (with free slip bottom), we find that changing the lower boundary to no slip reduces both the slab dip angle by 10–20°, and the trench retreat rate by a normalized velocity of ~0.0075. As also observed in the laboratory models, reducing the plate width to 600 km results in more rapid rates of trench retreat (by ~0.003 for the free slip cases) with no significant slow-down until the final phase of the model evolution. For the no slip models, we note that the effect of reducing the trench width on slab kinematics is greater than in the free slip models. For example, reducing the trench width from 1,800 to 600 km in the no slip models causes an increase in the normalized rate of trench retreat by an average of ~0.0075 (relative to ~0.003 in the free slip cases). Regarding the dynamic pressure in the mantle, we find that both narrow trenches and a free-slip lower boundary induce a lower across-slab pressure difference, with a more rapid change during the final phase of the models (Figures 4c and 4d).

3.3. Asymmetrical Double-Sided Subduction Models

3.3.1. Laboratory and Numerical Models With Geometric Asymmetry

We introduce an initial geometric asymmetry by starting the two opposing slabs of a homogeneous plate with different initial lengths. Here, we refer to the "faster side" as the side in which subduction is initiated

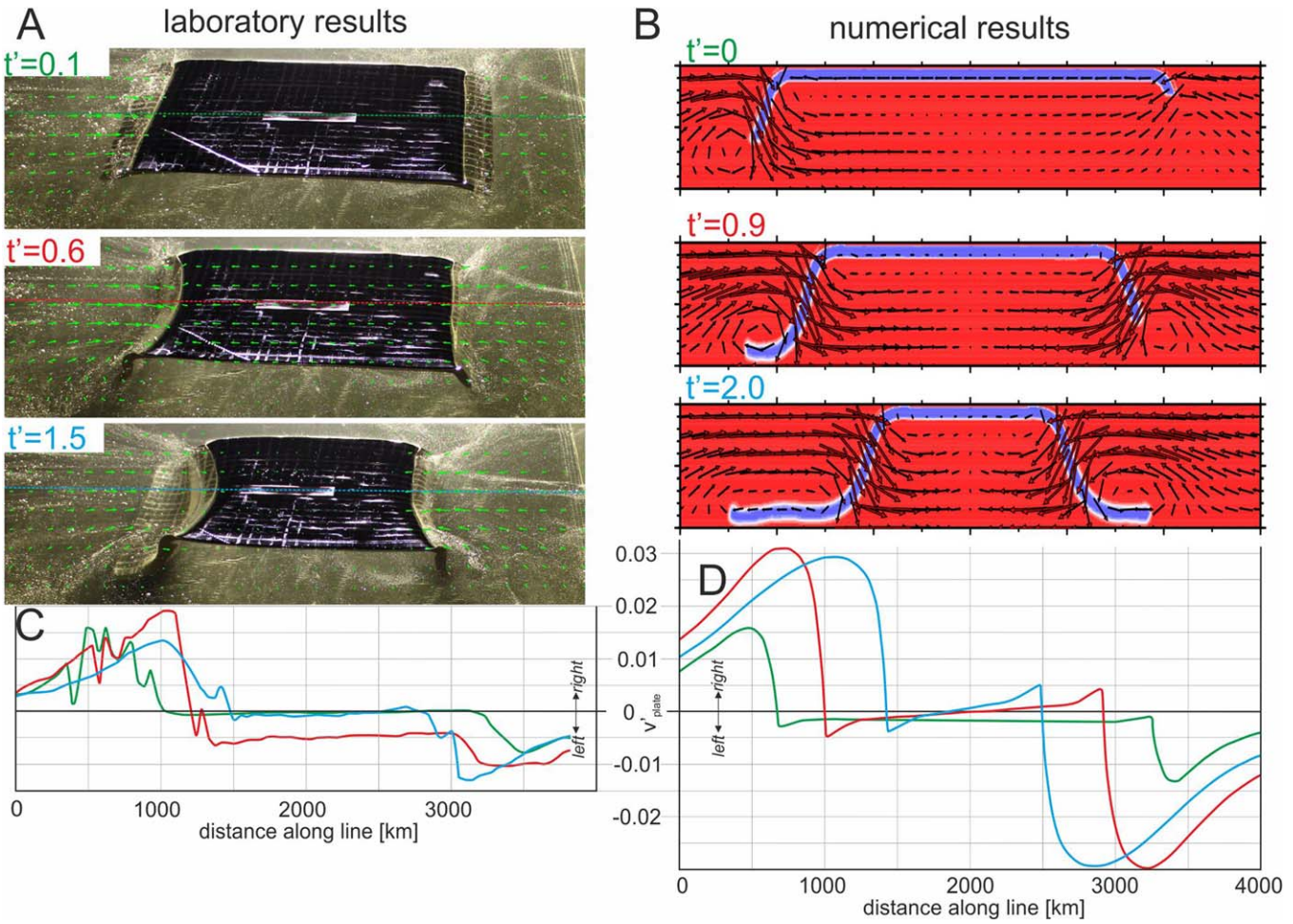

Figure 6. Plate movement during phase 1 due to the asymmetric start of subductions (geometric asymmetry). (a) Oblique-view photos from a laboratory model with surface velocities resulted from PIV analysis, where the subduction on the left is started with a longer initial slab. (b) Lateral view figures from the numerical model with similar geometric asymmetry, showing the mantle flow on a vertical plane. (c and d) Plate and mantle velocities along the centerline of the plate in the three time steps of the laboratory and numerical model, respectively. The times are normalized by the average time needed for the two slab to reach the bottom boundary.

by an initial slab length of 4 cm (240 km in nature) in the analog models and 400 km in the numerical model, while the "slower side" refers to the side with an initial slab length of 2.5 cm (150 km in nature) in the laboratory and 250 km in the numerical models. The asymmetrical initiation leads to net plate movement (toward the faster side) during the initial, free sinking phase, which then enforces the mantle flow on the forefront of the slower trench, thereby acting to equalize both the mantle circulation and the trench retreat velocity on the two sides of the plate (Figure 6). This feature is shown in both laboratory (Figure 6a) and numerical (Figure 6b) results. However, in the laboratory model with geometric asymmetry, the net plate movement is more rapid, resulting in a normalized plate velocity starting from 0.0009 (at t1 on Figure 6), peaking at 0.0050 (t2) and then decreasing to 0.0010 (t3). At the same time the normalized trench velocity changes from 0.0066 (t1) to 0.0078 (t2/t3) in the faster side, while in the slower side it is growing from 0.0010 (t1) to 0.0076 (t2/t3). In both modeling methods, the plate movement occurs early on in the evolution, when the resistive forces are smaller. Once the faster slab bends on the bottom of the model domain, the resistive forces are increased, and so the plate has less freedom to move and the double-sided subduction tends toward a symmetric evolution.

3.3.2. Laboratory Models With Mechanical Asymmetry

It follows from the preceding descriptions that, to reach an irregular double-sided subduction evolution, the setup needs to be changed to maintain an asymmetrical signature. Therefore, in the next part of the modeling study, we use heterogeneous plates to create mechanical asymmetry in the double-sided subduction

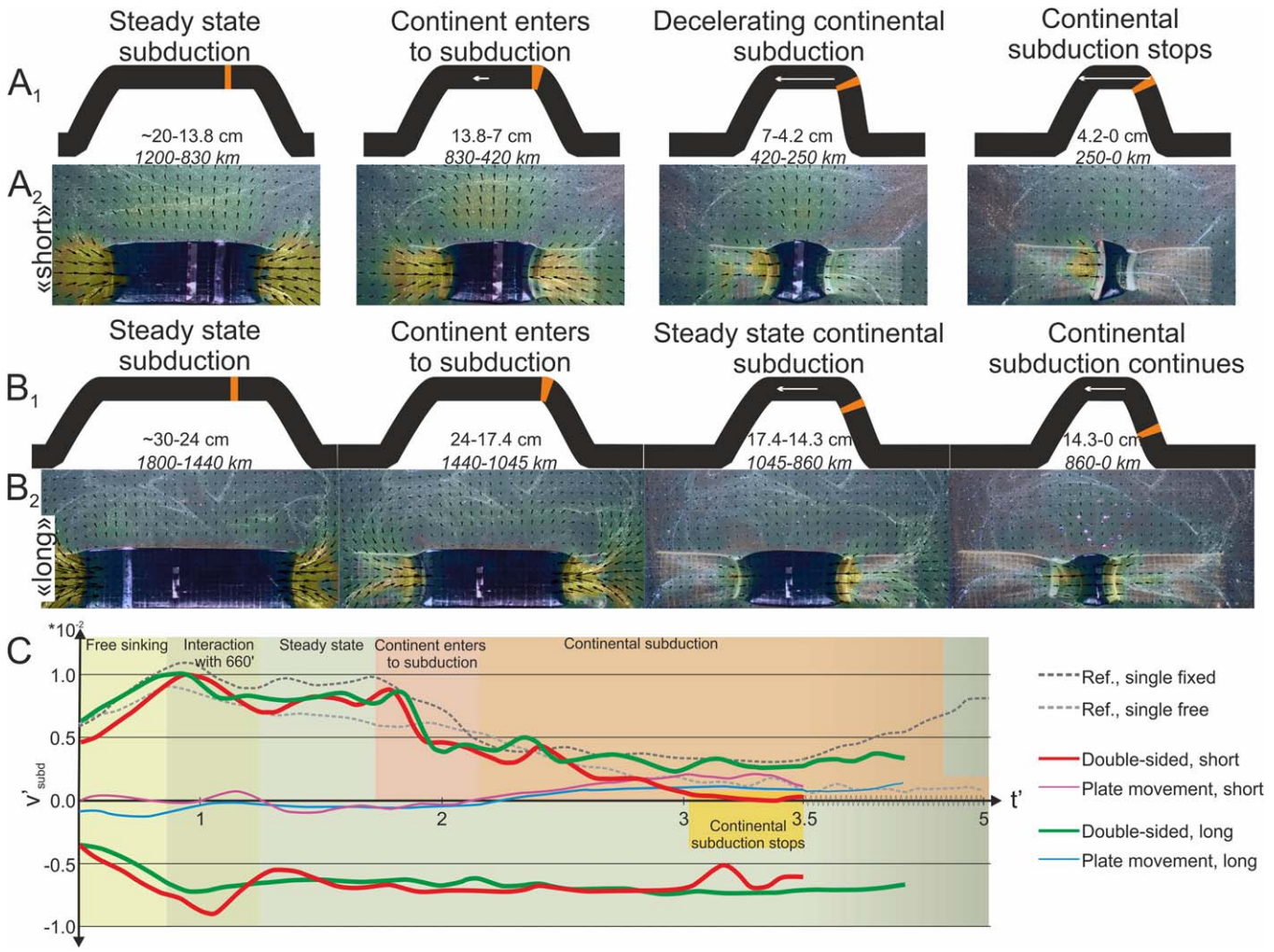

Figure 7. Evolution of (a) short and (b) long inhomogeneous models. 1, schematic figures of the characteristic phases with the trench distance and average plate movement; 2, top view photos and the mantle velocity. (c) Normalized subduction velocities of 10 cm wide single- and double-sided subductions. The thin lines show the plate velocity in the double models.

system. Similar to the inhomogeneous single slab reference model, the plate consists of an oceanic plate in which a 1 cm (=60 km) long continental stripe is embedded at a distance of 15 cm (=900 km) from one of the slab tips (Figure 2 and Table 2). Here we test two different plate widths (10 versus 30 cm) and two different initial plate lengths (40 versus 50 cm), to characterize the role of slab-slab interactions in the presence of mechanical heterogeneity. While the plate width has minimal effect on the models, the length of the plate plays a major role in the results of the experiments.

The double subduction process evolves as in the homogeneous double-sided model (section 3.2) until the onset of continental subduction at one of the trenches. When one of the trenches reaches the buoyant continental part, subduction dramatically slows down along the continental margin from 0.008 to 0.004 normalized subduction velocity, within only 2.7 cm (160 km) of convergence (Figure 7c). After this deceleration, the evolution of the partly continental subduction depends on the initial distance between the two trenches, which is either 40 or 50 cm in the short and long models, respectively (Table 2 and Figure 7). In the long plate model, a near-steady state behavior is reached shortly after continental subduction begins. In this case, the subduction attains a quasi-constant velocity around a normalized value of 0.003 until the end of the model. On the other hand, in the short model, after some stagnation, the slow-down of the partly continental subduction continues until subduction stops on the continental side, at a trench separation (Δx) of 3 cm (180 km). In both models, i.e., short and the long plate models, the oceanic subducting slabs evolve with similar trends, and at constant rates. However, the constant subduction rate is partly

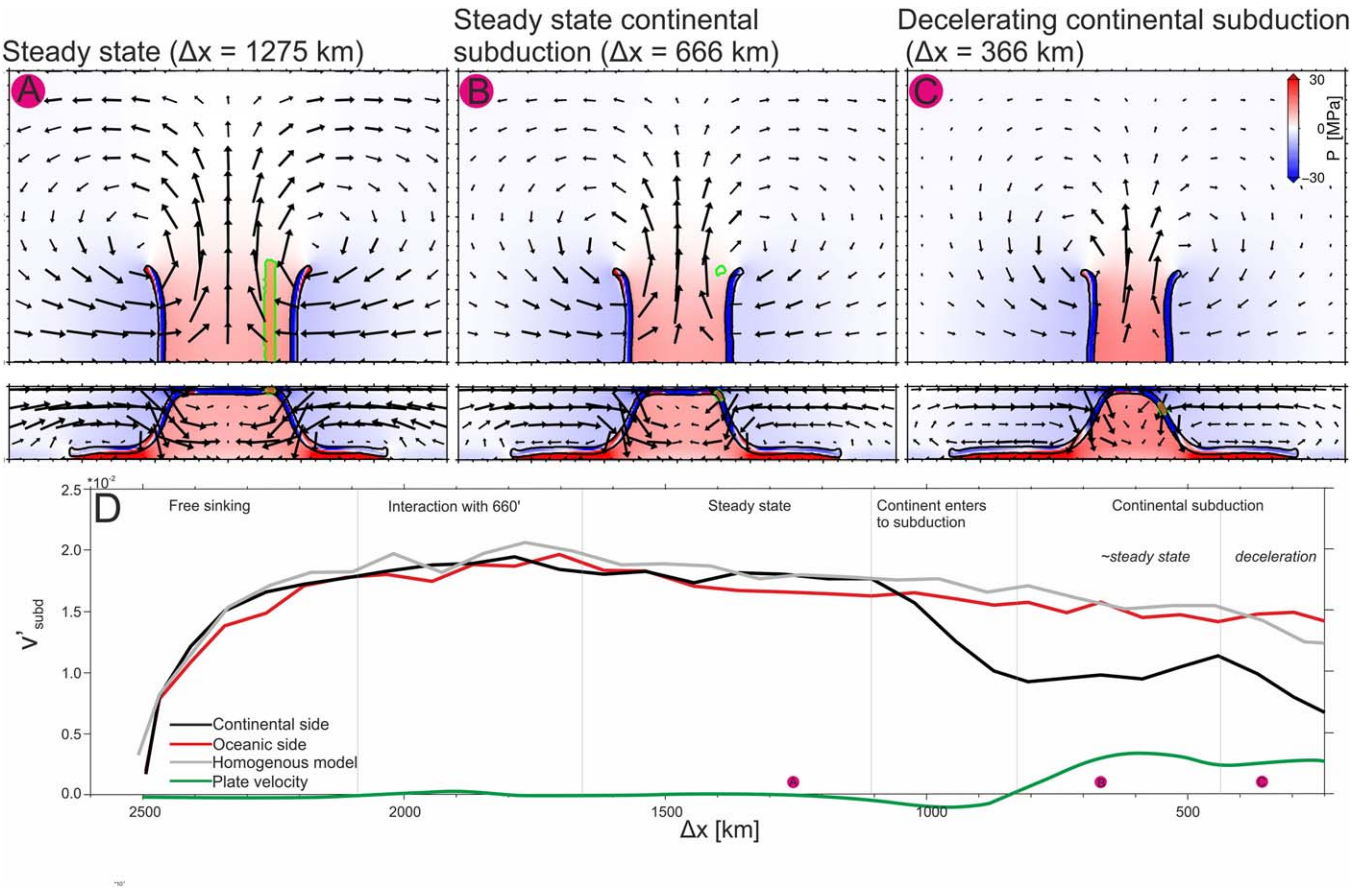

Figure 8. Evolution of subduction rate, mantle circulation, and subslab dynamic pressure for the inhomogeneous numerical model with a buoyant, continental strip. (a–c) Snapshots of the mantle flow and dynamic pressure fields taken at three representative times after the continent enters to the subduction zone. The horizontal slices (z = 330 km), and trench-perpendicular vertical slices taken at the center of the subducting plate (y = 0). (d) Evolution of normalized subduction velocity (= trench retreat rate + plate velocity).

accommodated by plate advance toward the pure oceanic subduction zone (Figure 7c), which balances the reduction of the oceanic trench retreat rate. It is noticeable that the net plate motion toward the faster subducting oceanic slab starts slightly earlier, and becomes larger, in the short model than in the long one (Figure 7).

Comparing the mantle flow induced in the homogeneous double-sided models (section 3.2) and the heterogeneous ones (Figures 3 and 7, respectively), the latter cases are characterized by a marked asymmetry of the, dominantly toroidal, escape flow. This asymmetry is coupled to the subduction of the continental stripe, mirroring the resulting trends in trench velocity. The asymmetry is less pronounced in the long plate model where the continental subduction plays a relatively minor role in the behavior of the system.

3.3.3. Numerical Models With Mechanical Asymmetry

The numerical setup of the asymmetric model is equivalent to the homogenous wide plate model, with a free slip base (section 3.1.3), but with the addition of a 60 km wide strip of buoyant continental lithosphere with a depth-averaged excess density of 40 kg/m^3 at 1,150 km distance from one of the slab tips (Table 1 and Figure 2). This model is therefore comparable to the long plate model described in the previous section (Figure 7b).

As in the laboratory model, the two subduction zones evolve symmetrically until the continental strip reaches the trench on one side of the system. When the continental strip initially reaches the trench, the two trenches are ≈1,100 km apart. At this time, the subduction rate at the trench undergoing continental subduction abruptly decreases, from a normalized value of ≈ 0.0175 to ≈ 0.0100, over ∼200 km convergence between the two trenches. Coupled with this reduction in subduction rate is a minor increase in the slab dip angle of around 4°, relative to the equivalent symmetric model with a homogeneous plate. As observed in the laboratory models, continental strip subduction triggers a net motion of the entire plate toward the purely oceanic trench, with a maximum normalized rate of ∼0.0030 (Figure 8d).

As continental subduction occurs at one trench, the other (purely oceanic) slab experiences a minor reduction in the trench retreat rate, relative to the symmetric case (section 3.2). This oceanic trench retreat rate reduction is, however, largely balanced by net plate motion directed toward the oceanic trench, and so the subduction rate, which is the sum of the plate and trench motion rates, is very similar to that observed in the homogeneous/symmetric model (Figure 8d). This simultaneous reduction in trench retreat velocity and increase in plate velocity at the oceanic trench is in strong agreement with the laboratory results described in the previous section.

Examining the model pressure field, we find that the subduction of the continental strip is associated with a decrease in the magnitude of the across-slab mantle pressure difference ΔP (by $\approx$ 4 MPa), and thereby a reduction in the magnitude of the associated, wedge-directed force, F_{dp}. Relative to the symmetric reference, a minor pressure reduction (1–2 MPa) occurs also across the purely oceanic slab in the asymmetric model, presumably in response to the net plate motion toward this trench that occurs in response to continental subduction.

4. Discussion

The modeling results presented above give new insights on the mechanisms of outward dipping double-sided subduction and support the interpretation of similar natural cases.

The laboratory reference, single subduction models are comparable with previous modeling results, confirming the presence of the three dynamic stages of subduction (Funiciello et al., 2003, 2004; Schellart, 2004), the mantle flow pattern around the slab edges (e.g., Funiciello et al., 2006; Piromallo et al., 2006; Strak & Schellart, 2014), and the effects of continental subduction (Espurt et al., 2008; Martinod et al., 2005, 2013a). Slight discrepancies can be attributed to the differences in the investigated parameter spaces. The homogeneous double-sided subduction models show a symmetric evolution, in accordance with previous numerical results (Di Leo et al., 2014; Holt et al., 2017). Furthermore, independent of initial geometric asymmetries, the symmetry of the system is obtained after both slabs reach the bottom boundary, which means that the system is self-stabilizing. However, when mechanical heterogeneities are included in the setup, the evolution departs from this simple case illustrating the relevant role of slab interaction, as previously shown by Zhang et al. (2017).

In this work, the laboratory and numerical modeling efforts corroborate and complement each other, leading to a more comprehensive understanding of how subduction zones interact. Regarding the first-order evolution of the subduction zones and the mantle flow patterns, the two modelling methods exhibit strongly comparable results. Quantitatively speaking, the numerical models systematically produce velocities that are about 40% higher than those within the laboratory models. This difference is likely due to the 15 km thick low viscosity crustal layer in the numerical model, which does not take part in the bending resistance. According to our estimate (based on Conrad & Hager, 1999) this can give 20% difference in the normalized velocity at the trench which doubles once the slab bends on the bottom of the box. Another important difference between the laboratory and numerical models is the surface tension, which slows down the experimental subduction rates considerably. While many researchers consider surface tension as an important factor in the analog studies (e.g., Jacoby, 1976; Schellart, 2008), its quantitative effect is not yet resolved. Schellart (2008) states that according to the topography of the syrup around the trench, the surface tension is comparable to the effect of including overriding and lateral plates around the slab. Variation in boundary conditions at the top/bottom/side walls may also contribute to the increased rates in the numerical models. Although there is a discrepancy regarding the amplitudes of the normalized velocities (i.e., observed velocity divided by the characteristic velocity derived from Stokes equation; equation (1)), the velocity trends are comparable, particularly when the plate is wide (30 cm/1,800 km).

As far as the subduction induced mantle circulation is concerned, laboratory and numerical outcomes are in robust agreement. As expected (Di Leo et al., 2014), double-sided subduction systems show a different subduction-induced mantle circulation pattern than single subduction. While the poloidal flow in the mantle wedge area mirrors the behavior of the single slab models, clear differences occur in the sub-slab area, where the two poloidal cells interfere as subduction enters its last phase (i.e., when $\Delta x < \sim$500 km). This results in a switch of the mantle flow direction below the center of the subducting lithosphere, from dominantly upwelling to weak downwelling (Figures 3 and 5). Consequently, the subducting plate may have a

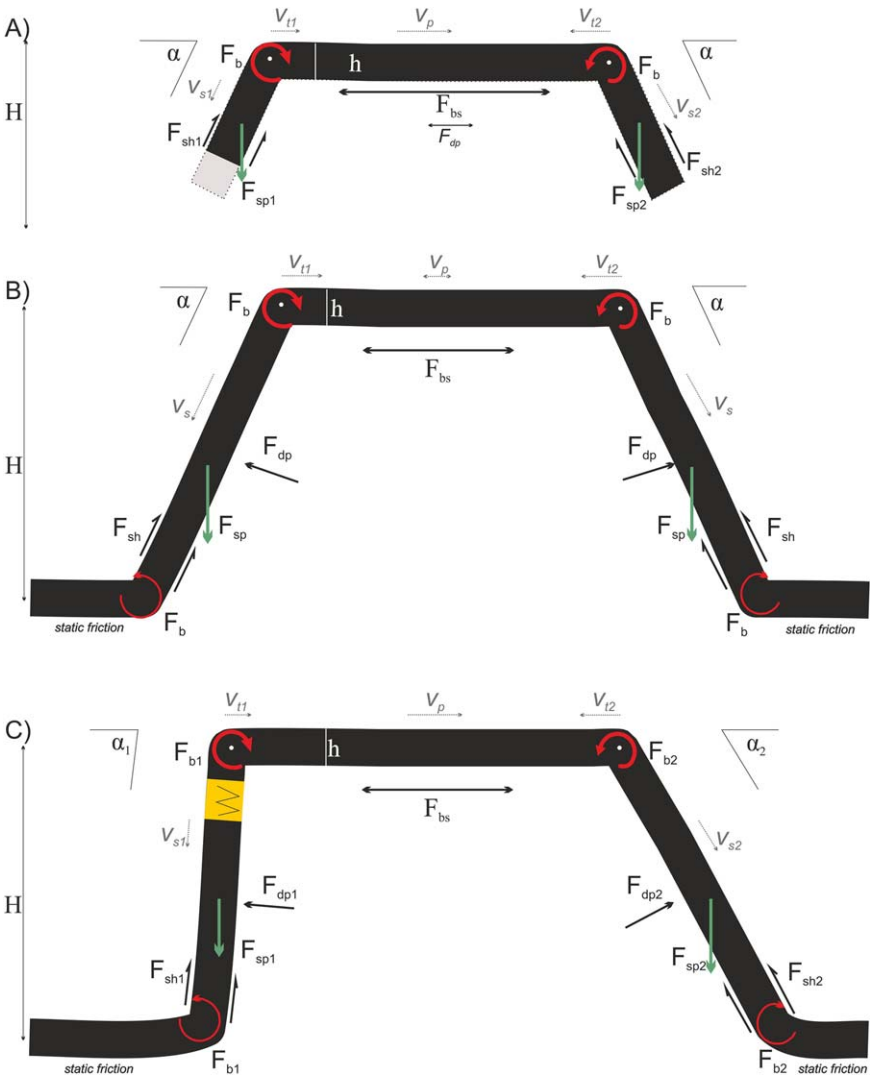

Figure 9. Forces in act during: (a) asymmetric subduction initiation; (b) symmetric subduction with approaching trenches; and (c) asymmetric subduction due to the presence of continental lithosphere. F_{sp}, slab pull force; F_{sh}, shear resistance on slab interface; F_{bs}, basal shear; F_{dp}, resistant force due to the increasing dynamic pressure; F_b, bending moment; v_s, subduction velocity; v_t, trench velocity; v_p, plate velocity; H, mantle thickness; h, lithospheric thickness; r, radius of curvature; α, angle of slab dip. In addition, a static friction is present between the slab and the bottom of the box. The plate itself has a finite viscosity; therefore, internal deformation (extension or compression) can happen in the lithospheric plate.

time dependent dynamic topography signal. A more significant discrepancy between double-sided- and single subduction systems is observable in the toroidal component of the induced mantle circulation. In single subduction models, the toroidal flow is concentrated around the edges of the slab and its strength is invariable during the steady-state phase reached after the slab interaction with the 660 km discontinuity. On the contrary, in double-sided subduction systems, the out-coming toroidal flow from the sub-slab area is observable all along the lateral sides of the subducting plate and has a time dependent behavior. As the two slabs approach each other, the sub-slab dynamic pressure increases driving a progressively increasing escape flow, which alters the shape of the toroidal cells from quasi-circular to elongated (Figure 3).

Three key scenarios describe the evolution of the double-sided subduction models, where slab interactions cause variations in slab geometry, trench/plate motions, and mantle circulation: A) symmetric versus asymmetric subduction initiation; B) symmetric subduction; and C) asymmetric subduction due to the presence of continental lithosphere. In the following section, we describe these three scenarios in the context of a simplified dynamic view (Figure 9). Finally, we speculate on the implications that the modeling results might have on natural cases.

4.1. The Impact of Initial Subduction Depth on Slab Pull Balance

Generally, in the homogenous models, the slab pull force is equal on the two sides of the system throughout the model evolution (dashed line on Figure 9a). The equivalent and progressively increasing slab pull forces on the two sides ($F_{sp1}=F_{sp2}$) are compensated by slab bending along its length ($R_{b1}=R_{b2}$) and the lithosphere-mantle shear resistance ($F_{sh1}=F_{sh2}$, F_{bs}). As a result, the initial phase of a homogeneous double subduction system is characterized by increasing trench retreat, subduction and mantle flow velocities, in analogy with the behaviour of a single subduction system (Funiciello et al., 2003, 2004; Schellart, 2004; Strak & Schellart, 2014).

However, an asymmetric initiation of the two subduction zones (i.e., geometric asymmetry) results in slabs reaching different depths at the same time. Because the slab pull force is linearly proportional to the length of the slab, this results in different slab pull forces on the two sides of the plate (Figure 9a). In this case, the dynamics of the system is tuned by the competition between the different slab pull forces (F_{sp2}-F_{sp1}), and the shear resistance forces on both the interfaces of the two slabs and on the bottom of the plate. The slab pull difference drives unequal trench retreat and subduction rates, accompanied by asymmetric flow velocities in the mantle wedge area and around the slab edges. Most importantly, since the slabs are not yet anchored at the 660 km discontinuity, the differential slab pull force is large enough to overcome the mantle resistance and result in net motion of the plate. The plate moves toward the faster subduction zone, enforcing the mantle flow in front of the slower slab, in the mantle-wedge area, which helps to equalize the subduction rate on the two sides (Figure 6a). Therefore, the interaction is achieved by stress transfer from one subduction zone to the other through the lithosphere. This implies that the subduction zones can interact via lithospheric stress transfer, even when there is a large distance between two subduction zones (i.e., $\Delta x > 1{,}000$–$1{,}500$ km). This is in agreement with previous results suggesting that, because lithospheric plates are relatively rigid, stress propagation is instantaneous and it can occur across the entire plate (Faccenna et al., 2012; Lithgow-Bertelloni & Guynn, 2004). On the other hand, stress transmission from the slab to the plate depends on the bending resistance of the plate, which on average consumes 20–30% of the slab pull force (Capitanio et al., 2009).

4.2. Increasing the Dynamic Pressure During Symmetric Evolution

During steady state subduction of the slabs in the homogenous double slab models, the slab pull force is ideally the same on the two sides of the system, and compensated by the slab bending and the lithosphere-mantle shear resistance (Figure 9b).

In the laboratory models, the slab dip angle and the trench retreat velocity at the two opposite subduction zones have values between the two end-member reference models with free and fix trailing edge conditions (Figure 3). The lateral migration (i.e., roll-back) of the slabs controls the circulation around the slab edges, producing patterns that differ from those observed in the single subduction case. Our experiments show that the poloidal flow in the mantle wedges of a double subduction is similar to that of a single slab system, in agreement with Di Leo et al. (2014). On the contrary, in the sub slab domain, the poloidal flow becomes weaker. Here, due to the increasing positive dynamic pressure, the mantle is driven to escape from below the plate, deforming the toroidal cells into a more elongated shape, and forming sub-slab mantle anisotropy parallel to the trench (Di Leo et al., 2014). As slabs approach, the asthenosphere in between becomes tightly constrained and the dynamic pressure increases in the sub-slab domain (Holt et al., 2017, Figure 4c). This causes the escape flow to become stronger, while trench velocities slowly decrease. The dynamic pressure increases, and trench retreat rate decreases more rapidly when the plate is wider (Figures 3–5). When the two opposite trenches reach a separation distance of 9–8 cm, ~540–480 km in nature, the subduction steps into its final stage, where trench velocities decrease with a higher rate, and the sub-slab dynamic pressure increases with an accordingly higher rate, resulting in further acceleration of the lateral escape flow (Figures 3–5). Simultaneously, in the sub-slab area the vertical flow reverses direction, and the upwelling below the center of the plate switches to a weak downwelling (Figures 3 and 5). This range of ~9–8 cm/~540–480 km can be considered as a critical distance at which the behavior of the model switches, and the two subduction zones interact through the mantle. The characteristic distance found here corresponds to the effective size of the subduction induced mantle flow cell in the upper mantle (Király et al., 2017). Furthermore, it is consistent with the numerical results of Király et al. (2016) in which slab interactions through stresses propagated in the mantle were investigated, and a comparable distance $<$600 km is found, in spite of the different set up. Furthermore, Mériaux et al. (2015) found a similar, 500 km trench

perpendicular distance, in which the toroidal flow could distort a stable mantle plume. Therefore, we speculate that the final stage of outward dipping double-sided subduction evolution occurs in relation to the interaction of the toroidal flow cells associated with the two opposite slabs.

4.3. Unbalanced Slab Pull During "Steady State" Subduction

In the mechanically heterogeneous models, the subduction of continental lithosphere of different nature, i.e., buoyancy, causes asymmetric slab pull (Figure 9c). Integrating the buoyancy force along the slab, the 1 cm strip of light, continental lithosphere reduces the slab pull force by about 15%. Such a minor difference in the pull force at the two margins of the plate is enough to drive an asymmetric evolution.

As the continental strip starts to subduct, the decreasing slab pull prompts a slow-down of the partly-continental slab subduction (Figures 7c and 8d). In agreement with previous single slab models (Espurt et al., 2007; Martinod et al., 2005, 2013b), the general slowing down of the subduction motions on the continental side is coupled to slab dip steepening and lower mantle flux rates (Figures 7 and 8). At the same time, the purely oceanic subduction is not affected, and subduction rate and slab dip remain constant.

Following the fast, initial deceleration, coupled to the beginning of the continental subduction, the evolution of the long (50 cm) or short (40 cm) plate models begin to differ from around 2.5 normalized time, when the trench separation distance is 17 versus 7 cm (1,020 versus 420 km), respectively. From this point, the partly continental slab reaches a steady state subduction rate in the long plate double-sided model, whereas in the short plate double-sided model the subduction rate decreases progressively to a halt (Figure 7). On the other hand, the purely oceanic subduction margin follows a similar trend in both models, with constant subduction rate, but decreasing trench retreat rate. The increasing plate motion is observable both in the short and the long model, although it is slightly higher in the short plate model.

The results show that the entry of the continental strip into the trench only halts subduction in the short plate model (Figure 7). This suggests that, in addition to the positive buoyancy of the continental lithosphere, the resistance force derived primarily from the sub-slab dynamic pressure plays an important role in the dynamic evolution of the asymmetric double-sided subduction system. In the short model, the dynamic pressure becomes large enough to resist the partly continental subduction when the trench distance is smaller than $\sim$7 cm (scaled to 420 km) (Figure 7). This critical distance is somewhat smaller than what we found in the homogenous models (9–8 cm/540–480 km), which is reasonable, as the slower continental subduction is coupled with a more moderately increasing sub-slab dynamic pressure (e.g., Capitanio & Faccenda, 2012).

Additionally, with the two trenches approaching and the difference between the subduction rates increasing, the differential pull at the oceanic and continental margins overcomes the plate basal shear resistance, inducing an increasingly rapid net plate motion. In the long plate model, as well as in the equivalent numerical simulation, due to a larger trench distance, the dynamic pressure is smaller in the sub-slab area and the basal shear acting on the plate is larger. This results in (1) a minor decrease of subduction velocity associated with continental subduction, and therefore a deeper subduction of the continental stripe, and (2) reduced plate motions, which further help to drag down the continent.

The asymmetric subduction rates are accompanied by an asymmetric escape flow, which becomes progressively more vigorous around the oceanic subduction zone, as the trenches approach.

4.4. Implications for Natural Cases

While natural examples of double sided subduction zones are not common, it is possible to identify at least two, present-day cases which can be unraveled in light of the results obtained in this study: the Sulawesi-Philippine region in SE Asia with the Sangihe-Halamera system and the central Mediterranean with the Apennines-Dinarides system (Figure 1). The former system can be related to the experiments with geometrical asymmetry, and the latter to a system with mechanical asymmetry.

The Sangihe-Halamera system bounds the Molucca Sea plate in northern Sulawesi (e.g., Hall, 2002). This microplate is subducting westward at the Sangihe Trench and eastward at the Halmahera Trench. The two subduction zones are so close that their two fore-arc basins are colliding in the only arc–arc collision setting currently observable on the Earth (Jaffe et al., 2004). The short distance between the two subduction zones – $<$ 170 km – implies that the slabs can interact both through the mantle and the lithosphere. On the other

hand, this double-sided system is strongly asymmetric. The Sangihe Trench has been active for 20–30 Myr, accommodated at least 1,000 km of plate convergence, and contains the deepest slab of the Philippine mobile belt (Lallemand et al., 1998). Subduction has occurred at the Halmahera trench for ~10 Myr and about 300 km of plate convergence has occurred with a mean convergence rate of about 3 cm/yr (Lallemand et al., 1998). The differential slab pull force between the two sides (i.e., geometric asymmetry) likely moved the plate toward the subduction zone with more rapid convergence (Sangihe; subduction velocity 72 mm/yr; Heuret et al., 2011) and boosted the mantle circulation (Zhang et al., 2017). Under this condition, trench-parallel anisotropy in the Molucca Sea is significantly stronger close to the Sangihe trench, in response to the higher trench retreat rate and the mantle flowing outward and escaping the sinking microplate (Di Leo et al., 2012).

Following the breakup of the Pangea supercontinent, the closure of the Tethys Ocean resulted in a complex tectonic environment in the Mediterranean area, with continental and oceanic lithospheric fragments progressively wedged between the converging African and Eurasian plates. The present tectonic setting here has been established in the late Cenozoic, resulting from subduction of oceanic fragments and continental block collision. In this frame, Adria occurred as a double-sided subduction system, confined by the westward dipping Apennine slab and the eastward dipping Dinaride slab, separated by an intermediate continental foreland lithosphere (Kruse & Royden, 1994). Our results suggest that the two subduction zones – the Apennines and the Dinarides – have been dynamically connected, first by mutual forcing that occurred through the lithosphere, and later, when the two trenches approached to a distance of ~500 km, by interaction through the mantle. Reconstructions of the area show that this critical distance is gradually reached from North to South between 20 and 10 Myr, respectively (Faccenna et al., 2014a; Handy et al., 2015).

Thus, the tectonic evolution of Adria has been determined by the differential rate of subduction and trench retreat rates on the two sides of the system. In this frame, the subduction of neutrally buoyant lithosphere along the Dinarides, followed by the subduction of buoyant continental lithosphere and the subsequent tear faulting and slab breakoff along the central Apennines (e.g., Faccenna et al., 2014b; Rosenbaum et al., 2002; Salimbeni et al., 2013; Wortel & Spakman, 2000) resulted in mechanical asymmetries since about 25 Ma. We infer that the recent eastward Adria motions toward the Central-Dinarides observed by present-day GPS measurements (Bennett et al., 2008), is related to the greatly reduced slab pull on the Apennine side. However, slab detachment may play a large role in the recent dynamics of the Adria plate. Additionally, according to the modeling results, the double-sided subduction of Adria may affect a large area via the escaping mantle flow that is directed toward the Alps and the Pannonian Basin. While on the thick and rigid Alps, the effect may be narrowly focused at the junction between the Alps and the Apennines (Király et al., 2016; Vignaroli et al., 2008), in the weak and thin Pannonian basin it could drive part of the Miocene- present deformation and rotation of the basin.

Presently, the distance between the Hellenic and Calabrian arc is increasing toward the south. We speculate that this geometric configuration induces a slightly different escape flow pattern with more divergent outflow at the Southern end of the slab, which may actively deform and curve the smaller Calabrian slab (e.g., Boutelier & Cruden, 2008).

5. Conclusions

We use analog and numerical modeling to investigate the slab-slab interactions in an outward dipping double-sided subduction setting, where a plate has two opposite convergent margins. We analyze and compare subduction kinematics, mantle flow and dynamic pressure in a range of setups where the two subduction zones have equivalent properties, have a geometrical heterogeneity (i.e., slab length), or a mechanical (buoyancy) heterogeneity. The setups mimic the natural conditions where, respectively, neighboring oceanic subduction zones might initiate at different times and/or develop different depths of subduction, but also where continental lithosphere might be subducted into one of the two margins, respectively.

We determine two ways of interactions:

1. In the case of two slabs with equivalent properties, the subduction zones have a symmetric evolution and initially they do not affect each other. However, when the modeled trenches are closer than ~9–8 cm/~ 540–480 km, the system transitions into a new dynamic behavior in response to the interaction

between subduction zones, due to stress propagation via the mantle circulation around the slab edges, in agreement with previous estimates (Király et al., 2016) using a different subduction geometry. As the two toroidal mantle flow cells interact, the dynamic pressure further increases in the sub-slab area. In the homogenous models this slows down trench retreat by ∼20%.

2. In the case of heterogeneous lithospheric buoyancy, an un-equal slab pull force develops on the two sides of the plate, following the entrainment of a partly continental slab, which drives an asymmetric subduction evolution. In these models the stress propagates through the lithosphere from the faster oceanic subduction zone to the slower partly continental one. When the shear resistance stresses at the plate base are overcome, episodic motion of the entire plate ensues. The interaction through the lithosphere can happen also at large distances (i.e., more than 1,500–200 km), when slabs are in their free sinking phase. Additionally, when the trenches approach a critical distance, ∼420 km in nature, the pressure increase in the sub-slab area are enough to lead, in combination with the decreased slab pull, to the termination of the continental subduction.

These results add weight to recent studies that emphasize the importance of interactions between proximal slabs (Di Leo et al., 2014; Holt et al., 2017; Király et al., 2016; Zhang et al., 2017). In natural double-sided subduction zones, slabs do not always behave as single entities, but their evolutions are strongly linked to neighboring slabs through the lithosphere or the mantle, depending on the distance between the two subduction zones. The mantle flow associated with double-sided subduction implies that the two subduction zones may not only affect each other, but also the larger area surrounding them. In the Mediterranean, for example, the double-sided subduction of Adria may have a substantial effect on the Apennines and the Dinarides, as well as in the surrounding areas such as the Pannonian Basin.

Acknowledgments
The authors are grateful for D. Boutelier and the other anonymous reviewer for their constructive comments on the paper. The laboratory models were realized in the Laboratory of Experimental Tectonics, at the University of Roma Tre. We thank the original authors and CIG (geodynamics.org) for providing CitcomCU, as used for the numerical modeling component. Additional data are available in the supporting information, which is also available via the EPOS database platform (http://dataservices.gfz-potsdam.de/portal/).

References

Bellahsen, N., Faccenna, C., & Funiciello, F. (2005). Dynamics of subduction and plate motion in laboratory experiments: Insights into the "plate tectonics" behavior of the Earth. *Journal of Geophysical Research*, *110*, B01401. https://doi.org/10.1029/2004JB002999

Bennett, R. A., Hreinsdóttir, S., Buble, G., Bašić, T., Bačić, Ž., Marjanović, M., et al. (2008). Eocene to present subduction of southern Adria mantle lithosphere beneath the Dinarides. *Geology*, *36*(1), 3–6. https://doi.org/10.1130/G24136A.1

Boutelier, D., Schrank, C., & Cruden, A. (2008). Power-law viscous materials for analogue experiments: New data on the rheology of highly-filled silicone polymers. *Journal of Structural Geology*, *30*(3), 341–353.. https://doi.org/10.1016/j.jsg.2007.10.009

Boutelier, D. A., & Cruden, A. R. (2008). Impact of regional mantle flow on subducting plate geometry and interplate stress: Insights from physical modelling. *Geophysical Journal International*,. *174*(2), 719–732. https://doi.org/10.1111/j.1365-246X.2008.03826.x

Burkett, E. R., & Billen, M. I. (2009). Dynamics and implications of slab detachment due to ridge-trench collision. *Journal of Geophysical Research*, *114*, B12402. https://doi.org/10.1029/2009JB006402

Capitanio, F. A., & Faccenda, M. (2012). Complex mantle flow around heterogeneous subducting oceanic plates. *Earth and Planetary Science Letters*, *353–354*, 29–37.

Capitanio, F. A., Morra, G., & Goes, S. (2009). Dynamics of plate bending at the trench and slab-plate coupling. *Geochemistry, Geophysics, Geosystems*, *10*, Q04002. https://doi.org/10.1029/2008GC002348

Conrad, C. P., Hager, B. H. (1999). Effects of plate bending and fault strength at subduction zones on plate dynamics. *Journal of Geophysical Research*, *104*(B8), 17551–17571. https://doi.org/10.1029/1999JB900149

Davy, P., & Cobbold, P. R. (1991). Experiments on shortening of a 4-layer model of the continental lithosphere. *Tectonophysics*, *188*(1–2), 1–25. https://doi.org/10.1016/0040-1951(91)90311-F

Di Leo, J. F., Walker, A. M., Li, Z. H., Wookey, J., Ribe, N. M., Kendall, J. M., & Tommasi, A. (2014). Development of texture and seismic anisotropy during the onset of subduction. *Geochemistry, Geophysics, Geosystems*, *15*, 192–212. https://doi.org/10.1002/2013GC005032

Di Leo, J. F., Wookey, J., Hammond, J. O. S., Kendall, J. M., Kaneshima, S., Inoue, H., et al. (2012). Deformation and mantle flow beneath the Sangihe subduction zone from seismic anisotropy. *Physics of the Earth and Planetary Interiors*, *194–195*, 38–54. https://doi.org/10.1016/j.pepi.2012.01.008

Djajadihardja, Y. S., Taira, A., Tokuyama, H., Aoike, K., Reichert, C., Block, M., et al. (2004). Evolution of an accretionary complex along the north arm of the Island of Sulawesi, Indonesia. *Island Arc*, *13*(1), 1–17. https://doi.org/10.1111/j.1440-1738.2003.00403.x

Druken, K. A., Kincaid, C., Griffiths, R. W., Stegman, D. R., & Hart, S. R. (2014). Plume–slab interaction: The Samoa–Tonga system. *Physics of the Earth and Planetary Interiors*, *232*, 1–14. https://doi.org/10.1016/j.pepi.2014.03.003

Espurt, N., Baby, P., Brusset, S., Roddaz, M., Hermoza, W., Regard, V., et al. (2007). How does the Nazca Ridge subduction influence the modern Amazonian foreland basin? *Geology*, *35*(6), 515–518. https://doi.org/10.1130/G23237A.1

Espurt, N., Funiciello, F., Martinod, J., Guillaume, B., Regard, V., Faccenna, C., & Brusset, S. (2008). Flat subduction dynamics and deformation of the South American plate: Insights from analog modeling. *Tectonics*, *27*, TC3011. https://doi.org/10.1029/2007TC002175

Faccenda, M., & Capitanio, F. A. (2012). Development of mantle seismic anisotropy during subduction-induced 3-D flow. *Geophysical Research Letters*, *39*, L11305. https://doi.org/10.1029/2012GL051988

Faccenna, C., Becker, T. W., Auer, L., Billi, A., Boschi, L., Brun, J. P., et al. (2014a). Mantle dynamics in the Mediterranean. *Reviews of Geophysics*, *52*, 283–332. https://doi.org/10.1002/2013RG000444

Faccenna, C., Becker, T. W., Lallemand, S., & Steinberger, B. (2012). On the role of slab pull in the Cenozoic motion of the Pacific plate. *Geophysical Research Letters*, *39*, L03305. https://doi.org/10.1029/2011GL050155

Faccenna, C., Becker, T. W., Miller, M. S., Serpelloni, E., & Willett, S. D. (2014b). Isostasy, dynamic topography, and the elevation of the Apennines of Italy. *Earth and Planetary Science Letters*, *407*, 163–174. https://doi.org/10.1016/j.epsl.2014.09.027

Faccenna, C., Funiciello, F., Giardini, D., & Lucente, P. (2001). Episodic back-arc extension during restricted mantle convection in the Central Mediterranean. *Earth and Planetary Science Letters*, *187*(1–2), 105–116. https://doi.org/10.1016/S0012-821X(01)00280-1

Faccenna, C., Heuret, A., Funiciello, F., Lallemand, S., & Becker, T. W. (2007). Predicting trench and plate motion from the dynamics of a strong slab. *Earth and Planetary Science Letters*, *257*(1–2), 29–36. https://doi.org/10.1016/j.epsl.2007.02.016

Forsyth, D., & Uyeda, S. (1975). On the relative importance of the driving forces of plate motion. *Geophysical Journal of the Royal Astronomical Society*, *43*(1), 163–200.

Funiciello, F., Faccenna, C., & Giardini, D. (2004). Role of lateral mantle flow in the evolution of subduction systems: Insights from laboratory experiments. *Geophysical Journal International*, *157*(3), 1393–1406. https://doi.org/10.1111/j.1365-246X.2004.02313.x

Funiciello, F., Faccenna, C., Giardini, D., & Regenauer-Lieb, K. (2003). Dynamics of retreating slabs: 2. Insights from three-dimensional laboratory experiments. *Journal of Geophysical Research*, *108*(B4), 2207. https://doi.org/10.1029/2001JB000896

Funiciello, F., Moroni, M., Piromallo, C., Faccenna, C., Cenedese, A., & Bui, H. A. (2006). Mapping mantle flow during retreating subduction: Laboratory models analyzed by feature tracking. *Journal of Geophysical Research*, *111*, B03402. https://doi.org/10.1029/2005JB003792

Guillaume, B., Husson, L., Funiciello, F., & Faccenna, C. (2013). The dynamics of laterally variable subductions: Laboratory models applied to the Hellenides. *Solid Earth*, *4*(2), 179–200. https://doi.org/10.5194/se-4-179-2013

Guillaume, B., Moroni, M., Funiciello, F., Martinod, J., & Faccenna, C. (2010). Mantle flow and dynamic topography associated with slab window opening: Insights from laboratory models. *Tectonophysics*, *496*(1–4), 83–98. https://doi.org/10.1016/j.tecto.2010.10.014

Hall, R. (2002). Cenozoic geological and plate tectonic evolution of SE Asia and the SW Pacific: Computer-based reconstructions, model and animations. *Journal of Asian Earth Sciences*, *20*(4), 353–431. https://doi.org/10.1016/S1367-9120(01)00069-4

Handy, M. R., Ustaszewski, K., & Kissling, E. (2015). Reconstructing the Alps–Carpathians–Dinarides as a key to understanding switches in subduction polarity, slab gaps and surface motion. *International Journal of Earth Sciences*, *104*(1), 1. https://doi.org/10.1007/s00531-014-1060-3

Hayes, G. P., Wald, D. J., & Johnson, R. L. (2012). Slab1.0: A three-dimensional model of global subduction zone geometries. *Journal of Geophysical Research*, *117*, B01302. https://doi.org/10.1029/2011JB008524

Heuret, A., & Lallemand, S. (2005). Plate motions, slab dynamics and back-arc deformation. *Physics of the Earth and Planetary Interiors*, *149*(1–2), 31–51. https://doi.org/10.1016/j.pepi.2004.08.022

Heuret, A., Lallemand, S., Funiciello, F., Piromallo, C., & Faccenna, C. (2011). Physical characteristics of subduction interface type seismogenic zones revisited. *Geochemistry, Geophysics, Geosystems, v*, *12*, Q01004. https://doi.org/10.1029/2010GC003230

Holt, A. F., Becker, T. W., & Buffett, B. A. (2015). Trench migration and overriding plate stress in dynamic subduction models. *Geophysical Journal International*, *201*(1), 172–192. https://doi.org/10.1093/gji/ggv011

Holt, A. F., Royden, L. H., & Becker, T. W. (2017). The dynamics of double slab subduction. *Geophysical Journal International*, *209*(1), 250–265. https://doi.org/10.1093/gji/ggw496

Hubbert, M. K. (1937). Theory of scale models as applied to the study of geologic structures. *Bulletin of the Geological Society of America*, *48*(10), 1459–1520.

Jacoby, W. R. (1976). Paraffin model experiment of plate tectonics. *Tectonophysics*, *35*(1–3), 103–113. https://doi.org/10.1016/0040-1951(76)90031-7

Jadamec, M. A., & Billen, M. I. (2010). Reconciling surface plate motions with rapid three-dimensional mantle flow around a slab edge. *Nature*, *465*(7296), 338–341. https://doi.org/10.1038/nature09053

Jaffe, L. A., Hilton, D. R., Fischer, T. P., & Hartono, U. (2004). Tracing magma sources in an arc-arc collision zone: Helium and carbon isotope and relative abundance systematics of the Sangihe Arc, Indonesia. *Geochemistry, Geophysics, Geosystems*, *5*, Q04J10. https://doi.org/10.1029/2003GC000660

Jarrard, R. D. (1986). Relations among subduction parameters. *Reviews of Geophysics*, *24*(2), 217–284. https://doi.org/10.1029/RG024i002p00217

Kincaid, C., & Griffiths, R. W. (2003). Labolatory models of the evolution of the mantle during rollback subduction. *Nature*, *425*(6953), 58. https://doi.org/10.1038/nature01966.1

Kincaid, C., & Griffiths, R. W. (2004). Variability in flow and temperatures within mantle subduction zones. *Geochemistry, Geophysics, Geosystems*, *5*, Q06002. https://doi.org/10.1029/2003GC000666

Király, Á., Capitanio, F. A., Funiciello, F., & Faccenna, C. (2016). Subduction zone interaction: Controls on arcuate belts. *Geology*, *44*(9), 715–718. https://doi.org/10.1130/G37912.1

Király, Á., Capitanio, F. A., Funiciello, F., & Faccenna, C. (2017). Subduction induced mantle flow: Length-scales and orientation of the toroidal cell. *Earth and Planetary Science Letters*, *479*, 284–297.

Kruse, S. E., & Royden, L. H. (1994). Bending and unbending of an elastic lithosphere: The Cenozoic history of the Apennine and Dinaride foredeep basins. *Tectonics*, *13*(2), 278–302. https://doi.org/10.1029/93TC01935

Lallemand, S., Popoff, M., Cadet, J.-P., Bader, A.-G., Pubellier, M., Rangin, C., & Deffontaines, B. (1998). Genetic relations between the central and Southern Philippine Trench and Sangihe Trench. *Journal of Geophysical Research*, *103*(B1), 933–950.

Lithgow-Bertelloni, C., & Guynn, J. H. (2004). Origin of the lithospheric stress field. *Journal of Geophysical Research*, *109*, B01408. https://doi.org/10.1029/2003JB002467

Long, M. D. (2013). Constraints on subduction geodynamics from seismic anisotropy. *Reviews of Geophysics, v*, *51*, 76–112. https://doi.org/10.1002/rog.20008

MacDougall, J. G., Kincaid, C., Szwaja, S., & Fischer, K. M. (2014). The impact of slab dip variations, gaps and rollback on mantle wedge flow: Insights from fluids experiments. *Geophysical Journal International*, *197*(2), 705–730. https://doi.org/10.1093/gji/ggu053

Martinod, J., Funiciello, F., Faccenna, C., Labanieh, S., & Regard, V. (2005). Dynamical effects of subducting ridges: Insights from 3-D laboratory models. *Geophysical Journal International*, *163*(3), 1137–1150. https://doi.org/10.1111/j.1365-246X.2005.02797.x

Martinod, J., Guillaume, B., Espurt, N., Faccenna, C., Funiciello, F., & Regard, V. (2013). Effect of aseismic ridge subduction on slab geometry and overriding plate deformation: Insights from analogue modeling. *Tectonophysics*, *588*, 39–55. https://doi.org/10.1016/j.tecto.2012.12.010

Mériaux, C. A., Duarte, J. C., Duarte, S. S., Schellart, W. P., Chen, Z., Rosas, F., et al. (2015). Capture of the Canary mantle plume material by the Gibraltar arc mantle wedge during slab rollback. *Geophysical Journal International*, *201*(3), 1717–1721. https://doi.org/10.1093/gji/ggv120

Moresi, L., & Gurnis, M. (1996). Dynamic Flow Models. *Earth and Planetary Science Letters*, *138*(1–4), 15–28.

Piromallo, C., Becker, T. W., Funiciello, F., & Faccenna, C. (2006). Three-dimensional instantaneous mantle flow induced by subduction. *Geophysical Research Letters*, *33*, L08304. https://doi.org/10.1029/2005GL025390

Porritt, R. W., Becker, T. W., & Monsalve, G. (2014). Seismic anisotropy and slab dynamics from SKS splitting recorded in Colombia. *Geophysical Research Letters*, *41*, 8775–8783. https://doi.org/10.1002/2014GL061958

Quinquis, M. E. T., Buiter, S. J. H., & Ellis, S. (2011). The role of boundary conditions in numerical models of subduction zone dynamics. *Tectonophysics*, *497*(1–4), 57–70. https://doi.org/10.1016/j.tecto.2010.11.001

Ranalli, G. (1995). *Rheology of the earth*. London, UK: Chapman and Hall.
Rosenbaum, G., Lister, G. S., & Duboz, C. (2002). Reconstruction of the tectonic Reconstruction of the tectonic evolution of the western Mediterranean since the Oligocene. *Journal of Virtual Exploration*, *8*, 107–126.
Salimbeni, S., Pondrelli, S., & Margheriti, L. (2013). Hints on the deformation penetration induced by subductions and collision processes: Seismic anisotropy beneath the Adria region (Central Mediterranean). *Journal of Geophysical Research: Solid Earth*, *118*, 5814–5826. https://doi.org/10.1002/2013JB010253
Schellart, W. P. (2004). Kinematics of subduction and subduction-induced flow in the upper mantle. *Journal of Geophysical Research*, *109*, B07401. https://doi.org/10.1029/2004JB002970
Schellart, W. P. (2008). Kinematics and flow patterns in deep mantle and upper mantle subduction models: Influence of the mantle depth and slab to mantle viscosity ratio. *Geochemistry, Geophysics, Geosystems*, *9*, Q03014. https://doi.org/10.1029/2007GC001656
Stegman, D. R., Freeman, J., Schellart, W. P., Moresi, L., & May, D. (2006). Influence of trench width on subduction hinge retreat rates in 3-D models of slab rollback. *Geochemistry, Geophysics, Geosystems*, *7*, Q03012. https://doi.org/10.1029/2005GC001056
Strak, V., & Schellart, W. P. (2014). Evolution of 3-D subduction-induced mantle flow around lateral slab edges in analogue models of free subduction analysed by stereoscopic particle image velocimetry technique. *Earth and Planetary Science Letters*, *403*, 368–379. https://doi.org/10.1016/j.epsl.2014.07.007
Strak, V., & Schellart, W. P. (2016). Control of slab width on subduction-induced upper mantle flow and associated upwellings: Insights from analog models. *Journal of Geophysical Research: Solid Earth*, *121*, 4641–4654. https://doi.org/10.1002/2015JB012545
Thielicke, W., & Stamhuis, E. J. (2014). PIVlab––Towards user-friendly, affordable and accurate digital particle image velocimetry in MATLAB. *Journal of Open Research Software*, *2*(1), e30. https://doi.org/10.5334/jors.bl
van Dinther, Y., Morra, G., Funiciello, F., & Faccenna, C. (2010). Role of the overriding plate in the subduction process: Insights from numerical models. *Tectonophysics*, *484*(1–4), 74–86. https://doi.org/10.1016/j.tecto.2009.08.038
Vignaroli, G., Faccenna, C., Jolivet, L., Piromallo, C., & Rossetti, F. (2008). Subduction polarity reversal at the junction between the Western Alps and the Northern Apennines, Italy. *Tectonophysics*, *450*(1–4), 34–50. https://doi.org/10.1016/j.tecto.2008.10.01
Weijermars, R., & Schmeling, H. (1986). Scaling of Newtonian and non-Newtonian fluid dynamics without inertia for quantitative modelling of rock flow due to gravity (including the concept of rheological similarity). *Physics of the Earth and Planetary Interiors*, *43*(4), 316–330. https://doi.org/10.1016/0031-9201(86)90021-X
Wortel, M. J., & Spakman, W. (2000). Subduction and slab detachment in the Mediterranean-Carpathian region. *Science (New York, N.Y.)*, *290*(5498), 1910–1917. https://doi.org/10.1126/science.290.5498.1910
Yamato, P., Husson, L., Braun, J., Loiselet, C., & Thieulot, C. (2009). Influence of surrounding plates on 3D subduction dynamics. *Geophysical Research Letters*, *36*, L07303. https://doi.org/10.1029/2008GL036942
Zhang, Q., Guo, F., Zhao, L., & Wu, Y. (2017). Geodynamics of divergent double subduction: 3-D numerical modeling of a Cenozoic example in the Molucca Sea region, Indonesia. *Journal of Geophysical Research: Solid Earth*, *122*, 3977–3998. https://doi.org/10.1002/2017JB013991
Zhong, S. (2006). Constraints on thermochemical convection of the mantle from plume heat flux, plume excess temperature, and upper mantle temperature. *Journal of Geophysical Research*, *111*, B04409. https://doi.org/10.1029/2005JB003972